Express Polymer Letters Vol.19, No.12 (2025) 1286–1309 Available online at www.expresspolymlett.com https://doi.org/10.3144/expresspolymlett.2025.95



Research article

# Sustainable polypropylene/tire rubber crumbs blends containing two flame retardant systems intended for the automotive industry

Sandra Paszkiewicz<sup>1,2\*®</sup>, Kamila Sałasińska<sup>3\*®</sup>, Zaida Ortega<sup>4®</sup>, Mateusz Barczewski<sup>5®</sup>, Jacek Andrzejewski<sup>5®</sup>, Konrad Walkowiak<sup>1®</sup>, Izabela Irska<sup>1®</sup>, Magdalena Jurczyk Kowalska<sup>3®</sup>, Anna Boczkowska<sup>3®</sup>, Marcin Borowicz<sup>6®</sup>, Joanna Paciorek-Sadowska<sup>6®</sup>, Elżbieta Piesowicz<sup>1,2®</sup>, Katarzyna Pokwicka-Croucher<sup>2</sup>

Received 11 June 2025; accepted in revised form 11 October 2025

Abstract. Two series of polymer blends based on post-consumer polypropylene (rPP) and tire rubber crumbs (Trc) under the trademark ECOPLASTOMER® PP70 with a mutual ratio of components 70/30 wt%, containing 10, 20, and 30 wt% of flame retardants, have been prepared using a twin-screw extruder. The influence of commercially available silane-treated alumina trihydrate (ATH-sil) with the eco-friendly system based on melamine phosphate (MP), aluminum hydroxide (AC), and peanut shells (PS), used as flame retardant agents, on the mechanical, thermal, and flammability properties of polymer blends was assessed – the incorporation of ATH-sil results in the appearance of peaks related to OH groups in the Fourier-transform infrared spectroscopy (FTIR) spectra. Similar observations are made for the MP/AC/PS system. differential scanning calorimetry (DSC) analysis revealed that using the selected flame retardants did not impact the melting and crystallization temperatures of the polymer. Tensile strength experienced a minor decrease, particularly in compositions containing more than 20 wt% of the flame retardants, while hardness remained unaffected by their share. Both flame retardants reduced the flammability of the modified polypropylene/rubber powder blends, and the most favorable outcomes were achieved with ATH-sil; however, only when employed at a minimum of 30 wt%. The formulated MP/AC/PS system proved more adept at reducing flammability and smoke emissions at lower flame retardant levels (up to 20 wt%).

Keywords: post-consumer materials, recycling, sustainability, flame retardant, mechanical properties, automotive industry

#### 1. Introduction

Plastic materials provide numerous benefits, including affordability, high toughness, durability, lightweight

properties, ease of processing, low thermal conductivity, and strong resistance to environmental factors and corrosion [1]. These advantages have driven a

<sup>&</sup>lt;sup>1</sup>West Pomeranian University of Technology, Faculty of Mechanical Engineering and Mechatronics, al. Piastow 19, 70-310 Szczecin, Poland

<sup>&</sup>lt;sup>2</sup>ECOPOLPLAST Sp. z o.o., ul. Chwaszczyńska 151E, 81-571 Gdynia, Poland

<sup>&</sup>lt;sup>3</sup>Warsaw University of Technology, Faculty of Materials Science and Engineering, Division of Ceramic Materials and Polymers, ul. Wołoska 141, 02-507 Warsaw, Poland

<sup>&</sup>lt;sup>4</sup>Universidad de las Palmas de Gran Canaria, Departamento de Ingeniería de Procesos, C. Juan de Quesada, 30, 35001 Las Palmas de Gran Canaria, Spain

<sup>&</sup>lt;sup>5</sup>Poznan University of Technology, Institute of Materials Technologies, Piotrowo 3, 61-138 Poznan, Poland

<sup>&</sup>lt;sup>6</sup>Kazimierz Wielki University in Bydgoszcz, Department of Chemistry and Technology of Polyurethanes, ul. J. K. Chodkiewicza 30, 85-064 Bydgoszcz, Poland

<sup>\*</sup>Corresponding author, e-mail: <a href="mailto:spaszkiewicz@zut.edu.pl">spaszkiewicz@zut.edu.pl</a> (Sandra Paszkiewicz) (Kamila Sałasińska) (Kamila Sałasińska)

steady increase in global plastic production since the 1950s, with annual primary production projected to reach 1100 million tons by 2050 if past trends from the last 70 years persist [2]. The widespread use of plastics has resulted in the rapid depletion of fossil fuel resources and the accumulation of large quantities of plastic waste. With over 90% of plastics produced from virgin fossil-based feedstocks, it is estimated that by 2050, the plastics industry will consume 20% of the total oil supply [3]. Effective management of plastic waste is crucial, as projections indicate that by 2050, 12000 million tons will accumulate in landfills or the natural environment due to plastics' slow degradation under ambient conditions [4]. Transitioning to a circular economy, where plastics are systematically reused, recycled, or recovered, is thus essential to mitigating the environmental impact of plastic waste [5]. Packaging represents the most extensive application of plastics and is responsible for approximately 70% of all plastic waste generated globally [5]. Among the most common plastics used in packaging, one can find polypropylene (PP), the polyolefin chosen for this work. Moreover, the largest share of polymers used in car production between 2016 and 2020 was polypropylene (44%) [6], due to its low cost, excellent processability, and good mechanical properties. However, herein we will focus mainly on the former mechanical recycling and the upcycling possibilities of post-consumer polyolefin-based PP materials, blending them with tire rubber crumbs, which were further modified to obtain new sustainable materials intended for automotive applications. It is an especially promising venture, since the transition towards higher circularity increased significantly between 2018 and 2022 [7]. However, more efforts are needed, considering the plastics sector is more than halfway towards achieving the roadmap ambition of 25% circular plastics by 2030. Many manufacturers are increasingly using recycled materials from internal circulation and redefining sustainability by deliberately introducing recycled materials, such as using over 30% recycled materials to manufacture the Renault Megane II as early as 2014 [8, 9].

Combining PP with rubber components like natural rubber (NR) or synthetic elastomers such as ethylene-propylene-diene monomer (EPDM) presents significant challenges due to the distinct nature of both components. The inherent mechanical properties of these blends have stimulated extensive research,

particularly concerning their structural integrity, thermal stability, and processing behavior. A primary challenge in blending PP with rubber is the reduction of mechanical strength due to rubber's soft nature and poor interfacial adhesion between the phases. This is further supported by studies showing the formation of less stable morphologies in blends with high rubber contents, where interfacial adhesion becomes critical [10].

Compatibility techniques have been proposed to overcome these issues. For instance, the introduction of compatibilizers such as maleic anhydride-grafted polypropylene (MAH-g-PP) has been shown to enhance interfacial adhesion in PP/rubber blends, thereby improving mechanical properties and reducing phase separation [11]. On the other hand, recent research has demonstrated that microstructural modifications can lead to substantial improvements. Li et al. [12] found that blending PP with core-shell rubber particles resulted in enhancements specifically in modulus, due to the better distribution and adhesion of the rubber phase within the matrix. This highlights the growing recognition of surface interactions and morphology as essential to achieving optimal performance in blends. In this sense, the Ecoplastomer PP70® addresses these challenges through advanced processing techniques, creating a material entirely from recycled sources without using additives or compatibilizers [13], which is the base polymer used in this research work. Similarly, recent studies emphasize sustainability by using recycled plastics and NR to create eco-friendly blends. Research by Martey et al. [14] highlights potential mechanical property improvements through the application of fillers (clay in this case) in blends of recycled PP and NR, thus addressing environmental concerns while enhancing material properties. As briefly outlined, the challenge in blending PP and rubber persists, particularly regarding mechanical properties and processability; moreover, the consideration of using flameretardant systems to reduce these materials' flammability remains unexplored.

As mentioned above, the use of polymer materials in the market is increasing exponentially due to their excellent properties, while their limited fire resistance poses a significant safety concern. Most polymeric materials are chemically composed of hydrocarbon chains, and when exposed to fire, they burn quickly, releasing large amounts of heat and smoke. [15, 16]. Therefore, the flammability of polymers has been

recognized as a social and scientific problem in many industries, including the automotive one [17]. The average automobile contains around 100 kg of plastic components, comparable to the energy equivalent of a full gasoline tank  $(3.10^9 \text{ J})$ . Automobile fires account for 95% of the 400 000 motor vehicle fires reported annually in the U.S., and are responsible for 92% of the 330 fire-related fatalities. Flammable plastics, including those in electrical wiring, upholstery, and various other components, represent the largest category of materials initially ignited in automobile fires (47%), followed by fuel, which accounts for 27% of ignitions [18]. On that account, improving flammability resistance in the automotive industry is crucial for safeguarding lives, meeting safety standards, enhancing public trust, and minimizing the impact of accidents on individuals and the environment. To address this issue, various additives, *i.e.*, phosphorus-based, nitrogen-based, mineral, carbon-based, bio-based, and hybrid flame retardants composed of two or more additives, have been explored to enhance their flame retardancy [19]. Flame retardants (FRs) are substances incorporated into flammable materials to prevent or slow down combustion, providing additional time for escape and increasing safety. These substances can be categorized into various classes, including halogenated compounds, phosphorusbased, nitrogen-based, intumescent systems, boronbased, silicon derivatives, inorganic substances, and natural substances [20, 21]. Halogenated compounds, such as chlorinated and brominated compounds, have historically been the most widely used flame retardants for plastics due to their high efficiency in disrupting the combustion process; however, environmental and health concerns have led to a decline in their use [21]. Consequently, regulations in Europe, such as REACH, WEEE, and RoHS, have been established to limit or even prohibit the use of many of these substances [22, 23]. Searching for alternative solutions is a significant challenge for the flame-retardant industry. An important group of non-halogen chemicals with flame-retardant properties is based on phosphorus compounds, particularly those known as intumescent FRs. These are increasingly popular due to their effectiveness in promoting the formation of a protective char layer on the material's surface, which insulates it from heat and reduces the spread of fire [24–27]. Melamine phosphate is especially valued for its nitrogen-phosphorus synergy, which enhances flame retardancy through mechanisms like char formation and the release of non-flammable gases [28–30]. Intumescent systems, which expand to form a protective barrier when exposed to heat, offer a practical solution, particularly in applications requiring high fire resistance [24, 31]. Another mechanism of action characteristic of inorganic substances, such as aluminum hydroxide and magnesium hydroxide, is that they release water vapor upon heating, cooling the material, and diluting combustible gases [32–35].

As the demand for sustainable solutions to waste management grows, the development of efficient technologies for recycling is critical to reducing environmental impact and conserving finite resources. In this study, a novel comparative approach by evaluating the performance of two flame retardant systems – commercial silane-treated alumina trihydrate (ATH-sil) and an innovative, eco-friendly formulation composed of melamine phosphate, boehmite, and peanut shell was presented. The proposed additives of natural origin, in the form of a mineral from the hydroxide group and waste from the food industry, were intended to replace some part of the synthetic FR and enhance its performance. The effectiveness of these solutions, as documented in the literature [36, 37], results in reduced product prices, increased waste valorization, and protection of nonrenewable resources. Since phosphate rock, from which all phosphorus-based chemicals are produced, is a limited resource, primarily located in China, the United States, Morocco, Russia, and Jordan, the EU introduced this resource, as well as elemental phosphorus, to the list of critical raw materials in 2014 and 2017, respectively. Sustainable management and improved recycling strategies are necessary globally to ensure that phosphate fertilizers and chemicals are preserved for future generations [37]. The work highlights the potential of bio-based and sustainable additives in enhancing recycled polymer composites' mechanical, thermal, and flame-retardant properties, offering a promising route toward greener, high-performance materials for demanding applications. The novelty stems from integrating sustainable flame retardants, the dual-system comparative approach, and the application to recycled polymer/rubber composites, offering scientific insight and practical relevance for automotive or building material applications. Efficient technology and applications for recycled waste have become increasingly essential to decrease environmental contamination and conserve nonrenewable resources. Therefore, this work aims to establish a comprehensive comparison between the commercially available silane-treated alumina trihydrate (ATH-sil) with the eco-friendly system based on peanut shells, melamine phosphate, and boehmite, used as flame retardant agents on the mechanical, thermal, and flammability properties of polymer blends consisted of postconsumer polypropylene (rPP) and tire rubber crumbs (Trc) with a mutual ratio of components 70/30 wt% under the trademark Ecoplastomer® PP70. Two materials based on PP70 containing 10, 20, and 30 wt% of flame retardants have been prepared using a twin-screw extruder. The chemical characterization of the compositions was analyzed using Fourier-transform infrared spectroscopy (FTIR) spectroscopy, while the structures were investigated using a scanning electron microscope (SEM). The compositions' mechanical properties, hardness, and melt flow index (MFI) have been assessed. Moreover, the thermal and thermomechanical properties have been studied using differential scanning calorimetry (DSC), thermogravimetric analysis (TGA), and Vicat/heat deflection temperature (HDT) and dynamic mechanical analysis tests, respectively. Finally, the flammability of the compositions has been analyzed using UL 94 and cone calorimetry (CC) measurements to select the system with the lowest flammability. Replacement of ATH-sil by the lignocellulose-based system should ultimately depend on the specific application requirements, including mechanical performance, cost efficiency, environmental considerations, and anticipated fire occurrence.

## 2. Materials and methods

#### 2.1. Materials

The polymer matrix used in this study was the blend of post-consumer polypropylene with Trc with a mutual ratio of components of 70% polypropylene and 30% Trc under the trademark Ecoplastomer® PP70 provided by Ecopolplast sp. z o.o. (Gdynia, Poland). According to manufacturer's data, PP70 has the following parameters: density 1 g/cm<sup>3</sup>; MFI: 22 g/10 min (230 °C/5 kg), tensile stress at yield: 16 MPa, tensile stress at break:16 MPa, elongation at break: 47%, Young's modulus: 381 MPa, Charpy Impact strength: 28 kJ/m<sup>2</sup>, hardness 62 Shore D. Moreover, it is an innovative thermoplastic elastomer made entirely of post-consumer recycled plastic and recycled tire rubber crumb that ensures complete independence from fossil fuels and significantly reduces environmental as well as CO<sub>2</sub> impact. The Trc used in Ecoplastomer® is obtained from recycled end-oflife tires from passenger cars and trucks. It is produced as a mixed feedstock of summer and winter tyres, processed together into a uniform material, and ground to a particle size of less than 1 mm. Moreover, their technology creates strong rubber and plastic bonding without chemical additives or stabilizers. The lack of additives makes the Ecoplastomers fully circular [13]. As flame retardants, one used the following materials presented in Table 1. The system's MP:AC:PS ratio was 3:2:0.5, while the total flame retardant share ranged from 10 to 30 wt%.

Table 1. Characterization of the flame retardants used.

Flame retardant	ATH-sil	MP	AC	PS
	Surface modified alumina	Melamine phosphate, Exflam	ACTILOX® B60 (Nabaltec,	Peanut shells (Arachis hy-
	trihydrate Apyral 40 VS1	MP (Wellchem Chemicals,	Schandorf, Germany) is a	pogaea L. species) were pro-
	(Nabaltec, Schandorf, Ger-	Zhejiang, China), with phos-	boehmite mineral-based	vided by local suppliers
	many), vinyl silane treated	phorus wt% of min. 12%, ni-	flame retardant, with 99%	(Poland, Central Europe),
		trogen wt % of 36–38%, den-		
	98.5% content of Al(OH) <sub>3</sub> ,	sity 1.74 g/cm <sup>3</sup> , particle size	ic surface area of 5.0 m <sup>2</sup> /g, a	conducted for 7 days at
	the specific surface area of	D50 of 10 μm	bulk density of 400 kg/m <sup>3</sup> ,	65±5 °C, while grinding on a
	3.5 m <sup>2</sup> /g, bulk density of		and a whiteness of 98%	laboratory sieve mill L-0210
Characterization	350 kg/m <sup>3</sup> , density of			from Cloer
Characterization	2.4 g/cm <sup>3</sup>			

#### 2.2. Preparation of the testing samples

Two PP70-based compositions were prepared using a counter-rotating twin-screw extruder (LSM30, Leistritz Laborextruder Extrusionstechnik GmbH, Nuremberg, Germany). Series I contained ATH-sil, while Series II consisted of the MP/AC/PS system. The extruder was equipped with intermeshing screws and interchangeable mixing sections (screw diameter D = 34 mm, L/D ratio = 23), as well as a set of gravimetric feeders for accurate dosing of the component proportion. Materials were dried in a dryer under a dynamic vacuum before extrusion. The temperature of the extrusion process was selected based on the DSC analysis for PP70 and the thermal degradation temperatures of the system containing, among others, peanut shells. Thus, the following parameters were determined for extruding PP70-based compositions: zone 1 (feed zone): 145 °C, zone 2: 165 °C, zone 3: 180°C, zone 4: 180°C, zone 5: 190°C, zone 6: 190 °C, zone 7: 190 °C, zone 8 (die): 190 °C. The rotational speed of the screws of 40 rpm. Yield: 2.0 kg/h. The obtained materials were pelletized and injection molded using Boy 35 (Dr BOY GmbH & Co., Neustadt, Germany) to obtain dumbbell shape samples, type ISO 37 type A3, for tensile measurements, for cone calorimetry measurements, polymer plagues with dimensions of 100×100×4 mm were prepared in accordance with the standard procedure (ISO 5660). Test specimens for the UL 94 flammability evaluation were prepared by compression molding into bars of 125×13×3 mm using the following conditions: phase 1: 190 °C/10 bar/60 s; phase 2: 190 °C/40 bar/120 s;

phase 2: 190 °C/40 bar/120 s phase 3: 150 °C/50 bar/70 s.

#### 2.3. Characterization methods

Attenuated total reflectance – Fourier transform infrared (ATR-FTIR) spectra of the analyzed materials were recorded using an FTIR spectrophotometer Perkin Elmer Two (Perkin Elmer, Waltham, MA, USA) with 64 scans and a resolution of 4 cm<sup>-1</sup> over the frequency range of 4000–400 cm<sup>-1</sup>.

The dispersion of the additives was investigated by field emission scanning electron microscopy (FE-SEM Hitachi SU-8000, Tokyo, Japan). Before the test, the samples were cryofractured in liquid nitrogen and then vacuum-coated with a thin gold film (EM ACE200, Leica, Wetzlar, Germany). Secondary electrons (notation SE in photographs) images using an acceleration voltage of 5 kV were acquired.

The differential scanning calorimetry (DSC) was performed using a DSC 204 F1 Phoenix (Netzsch, Selb, Germany) thermal calorimeter under a nitrogen atmosphere in the heating-cooling-heating cycle, with the heating/cooling rate of  $10\,^{\circ}$ C/min, from -85 to  $250\,^{\circ}$ C, and sample weight  $10\pm0.2$  mg. The crystallization temperature ( $T_{\rm c}$ ) and melting temperature ( $T_{\rm m}$ ) were determined from the maximum of the exothermic and endothermic peaks, respectively. The heat of fusion ( $\Delta H_{\rm m}$ ) and crystallization ( $\Delta H_{\rm c}$ ) were calculated from the total areas under melting and crystallization peaks on the DSC curve, considering the ratio of fillers for each formulation. The degree of crystallinity ( $X_{\rm c}$ ) was calculated using the Equation (1):

$$X_{\rm c} = \frac{\Delta H_{\rm m}}{\Delta H_{\rm m}^0 (1 - \alpha)} \tag{1}$$

where  $\Delta H_{\rm m}$  is the melt enthalpy,  $\Delta H_{\rm m}^0$  is the heat of fusion of 100% crystalline PP (207 J/g) and  $\alpha$  is the ratio of the used filler and/or additives [38].

The Vicat softening temperature (VST) and heat deflection temperature (HDT) were determined with a Testlab RV300C (Testlab, Warsaw, Poland) apparatus. Measurements were performed in an oil bath following the ISO 36 and ISO 75 standards. The VST measurement was conducted at a 50 °C/h heating rate and 50 N load. The HDT B-type experiment was prepared with a heating rate of 120 °C/h and a load of 1.8 MPa. The dynamic mechanical thermal analysis (DMA) test was performed using the Anton Paar MCR 301 rheometer (Graz, Austria) equipped with a torsion DMA measuring tool. Investigations were carried out with a constant frequency of 1 Hz and a strain of 0.01%. All samples were cooled to -100 °C and heated up to 120 °C with a temperature ramp of 3 °C/min. The effectiveness of the filler is based on the determination of the 'C-factor' according to the (Equation 2) [39]:

$$C = \frac{\frac{G_g'}{G_r'}|\text{composition}}{\frac{G_g'}{G_r'}|\text{matrix}}$$
 (2)

where  $G'_{\rm g}$  and  $G'_{\rm r}$  are the values of storage modulus in the glassy region (-80 °C) and rubbery region (80 °C), respectively. The thermal stability of materials was assessed under oxidizing conditions, using an air flow of 10 mL/min. The assessment was performed from 30 to 700 °C, with samples of 15 mg placed in alumina crucibles, in a Perkin Elmer TGA

400 apparatus (Perkin Elmer, Waltham, MA, USA). The exhaust gases were further analyzed by FTIR (TGA-FTIR) in a Perkin Elmer Spectrum 2 spectrophotometer (Perkin Elmer, Waltham, MA, USA). The spectra were collected along the entire heating cycle. The transfer line was set at 270 °C, and the measurement cell generated a gas flow of 70 mL/min.

Melt flow rate (MFR) measurement has been performed using A-MeP extrusion plastometer, Noselab ATS (Bovisio-Masciago MB, Italy). Tests were carried out according to the ISO 1133 standard at 230 °C and under a load of 2.16 kg.

The static mechanical properties were carried out using EZ-TEST-LX universal testing machine (Shimadzu, Kyoto, Japan) equipped with a 1 kN Shimadzu load cell, digital extensometer TRViewX-500D, and TRAPEZIUM X software. Tensile tests were performed at a crosshead speed of 25 mm/min to break at room temperature. The reported values are the mean values of five measurements. The measurements were performed according to PN-EN ISO 527. The rebound resilience was determined with a Schob-type pendulum Zwick 5109 (ZwickRoell GmbH & Co. KG, Ulm, Germany) in accordance with the ISO 4662 standard.

The Shore D hardness was measured using a manual Shore test stand, SAUTER TI (Freiburg, Germany). The reported values are an average of 10 independent measurements.

The reaction to a small flame was assessed using UL 94 measurements, and tests were conducted in accordance with EIC 60695-11-10. The specimens, with dimensions of 125×13×3 mm in vertical and horizontal orientations, were subjected to a 50 W flame. The

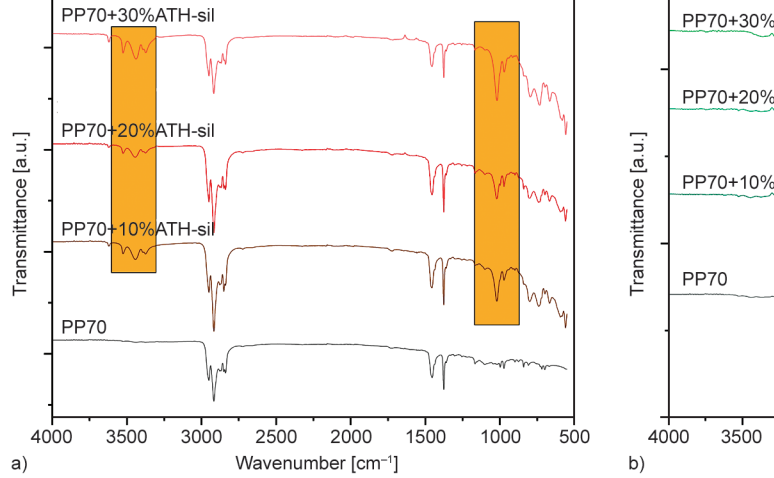
parameters evaluated were the burning time, the occurrence of burning drops, and the burning rate.

Using a cone calorimeter (Fire Testing Technology, East Grinstead, UK), measurements were performed following the ISO 5660 procedures, and the burning behavior of the investigated materials was assessed. The horizontally oriented samples were irradiated at a heat flux of 35 kW/m<sup>2</sup>, and spark ignition was employed to ignite the pyrolysis products. An optical system with a silicon photodiode and a helium-neon laser provided a continuous survey of smoke. Three tests were made for each series, and the residues were photographed using a digital camera as well as a metallographic microscope PANTHERA 2.0 (Motic Scientific Instruments, Barcelona, Spain) for observation in the bright and dark field in reflected light with a high-sensitivity microscope camera with a resolution of ~5.0 MP (2448×2048 pixels) (Motic Scientific Instruments, Barcelona, Spain). The obtained images were taken at 100× magnification. Each of the obtained microscopic images was a composite of multiple images in the Z axis. The registration and composite of microscopic images was performed using the Motic Images Plus 3.0 data acquisition and archiving program (Motic Scientific Instruments, Barcelona, Spain).

#### 3. Results and discussion

# 3.1. Structural properties and distribution of additives

The structure of PP70-based compositions containing two systems of flame retardants was investigated using FTIR spectroscopy (Figure 1). For the reference material (PP70), one could observe the absorption peak located at 840 cm<sup>-1</sup> assigned to C–CH<sub>3</sub>



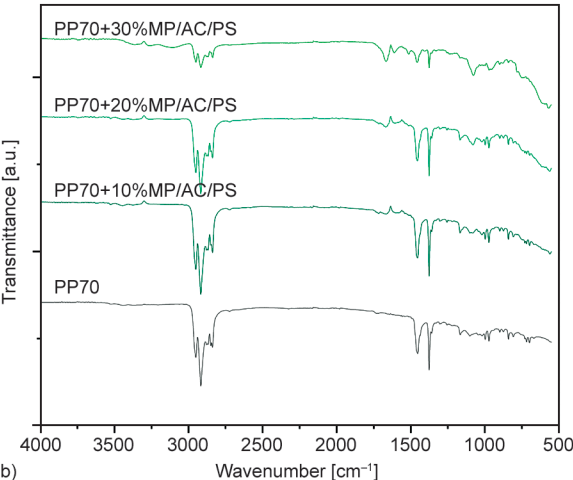


Figure 1. FTIR spectra of PP70-based compositions containing two systems of flame retardants. a) ATH-sil, b) MP/AC/PS.

stretching vibration, and absorption peaks displayed at 972, 997, and 1165 cm<sup>-1</sup> assigned to -CH<sub>3</sub> rocking vibration. In turn for all samples, both with the addition of ATH-sil and the MP/AC/PS system, the symmetric bending vibration mode of -CH<sub>3</sub> group at 1375 cm<sup>-1</sup>, absorption peak at 2952 cm<sup>-1</sup> related to -CH<sub>3</sub> asymmetric stretching vibration, as well as absorption peaks at 1455, 2838, and 2917 cm<sup>-1</sup> attributed to -CH<sub>2</sub>- symmetric bending, -CH<sub>2</sub>- symmetric stretching and -CH<sub>2</sub>- asymmetric stretching, respectively, were detected [40]. For ATH-sil samples, some significant differences can be observed compared to the PP70, attributed to the OH vibration in Al(OH)<sub>3</sub> (3621–3281 cm<sup>-1</sup>), which is more significant for the higher content in ATH in the final materials, together with the bands at 1020 and 796-566 cm<sup>-1</sup>, related to Al–O bonds [41, 42]. For the green IR system proposed, the most significant differences with the spectrum for the PP70 are in the appearance of a sharp peak at 1665 cm<sup>-1</sup> (P–O–H in melamine phosphate), 1077 cm<sup>-1</sup> (Al–O bonds in AC), and a wide band from 700-500 cm<sup>-1</sup> (P-O in MP and Al-O in AC) [26, 41, 43].

Dispersion of Trc and modifiers in a PP is instrumental in determining material properties. Thus, SEM was conducted to investigate the microstructure of the materials. The resulting micrographs are presented in Figure 2. The Trc is uniformly dispersed within the PP and appears as white rods in darkened PP. Furthermore, Trc are well embedded within the PP, and in regions where pull-out occurs due to fracture, they exhibit spherical and well-defined shapes. These observations indicate strong adhesion between the rubber crumbs and the polymer matrix. A similar relationship was reported for PP/EPDM [44], and PP/NR [45, 46].

The fracture surface of materials differs from the neat matrix, while the surface of the polymer is almost smooth; the incorporation of particles results in higher roughness. These surface flaws can be due to weak interface bonding between the polymer and the utilized flame retardants [47, 48]. The particles were evenly distributed within the polymer at ATH-sil concentrations of 10 and 20%. At a concentration of 30%, small aggregates of ATH-sil particles were observed; however, these agglomerates were still uniformly dispersed throughout the bulk polymer. The presence of visible interfacial gaps and voids between ATH-sil particles and the polymer indicates weak interfacial adhesion between these components

[48–50]. The weak adhesion is likely due to the incompatibility between the nonpolar polyolefin matrix and the hydrophilic ATH particles [50–52]. The MP/AC/PS additives were dispersed evenly at each share. Like the ATH-sil, the MP/AC/PS particles exhibit weak adhesion to the polymer, as evidenced by visible interfacial gaps and voids between the components. This phenomenon has been observed in multiple studies [28, 53]. Therefore, weak interfacial adhesion between the components can negatively affect mechanical performance, which will be discussed later.

#### 3.2. Thermal properties

Phase transition temperatures were investigated using DSC analysis. The DSC thermograms are presented in Figure 3. Since post-consumer PP, which was the basis for PP70, contained a small amount of polyethylene (PE), melting and crystallization peaks of PP and PE were expected in the thermograms. In fact, the phase transitions related to the melting of both polyolefins were detected and recorded during the heating process. The lack of differentiation of separate peaks originating from crystallization for two polyolefin varieties is due to the overlapping effects; similar results were reported in the work of Sutar et al. [54]. The melting temperature that comes from PP in PP70 was found to be 163 °C. Moreover, PP70 crystallized during cooling with a crystallization temperature of 121 °C. Observing the phase transition temperatures for both compositions with the addition of flame retardants, no significant changes in the melting and crystallization temperatures were noted (Table 2). The limited effect of the FRs' addition on  $T_{\rm m}$  and  $T_{\rm c}$  can be explained by phenomena already occurring in the polymer, which constitutes a complex system. However, for both series of compositions, a gradual decrease in the degree of crystallinity with increasing modifier content (from 10 to 30%), can be observed. This effect is most likely attributed to the reduction in the overall amount of crystalline polypropylene in the system. As the proportion of modifier increases, the relative content of PP, the phase responsible for crystallization, decreases. Furthermore, the presence of rubber and modifiers can interfere with the regular packing of PP chains, restricting chain mobility and hindering the formation of ordered crystalline regions. Consequently, both the reduction in crystallizable PP fraction and the disturbance of crystal growth contribute

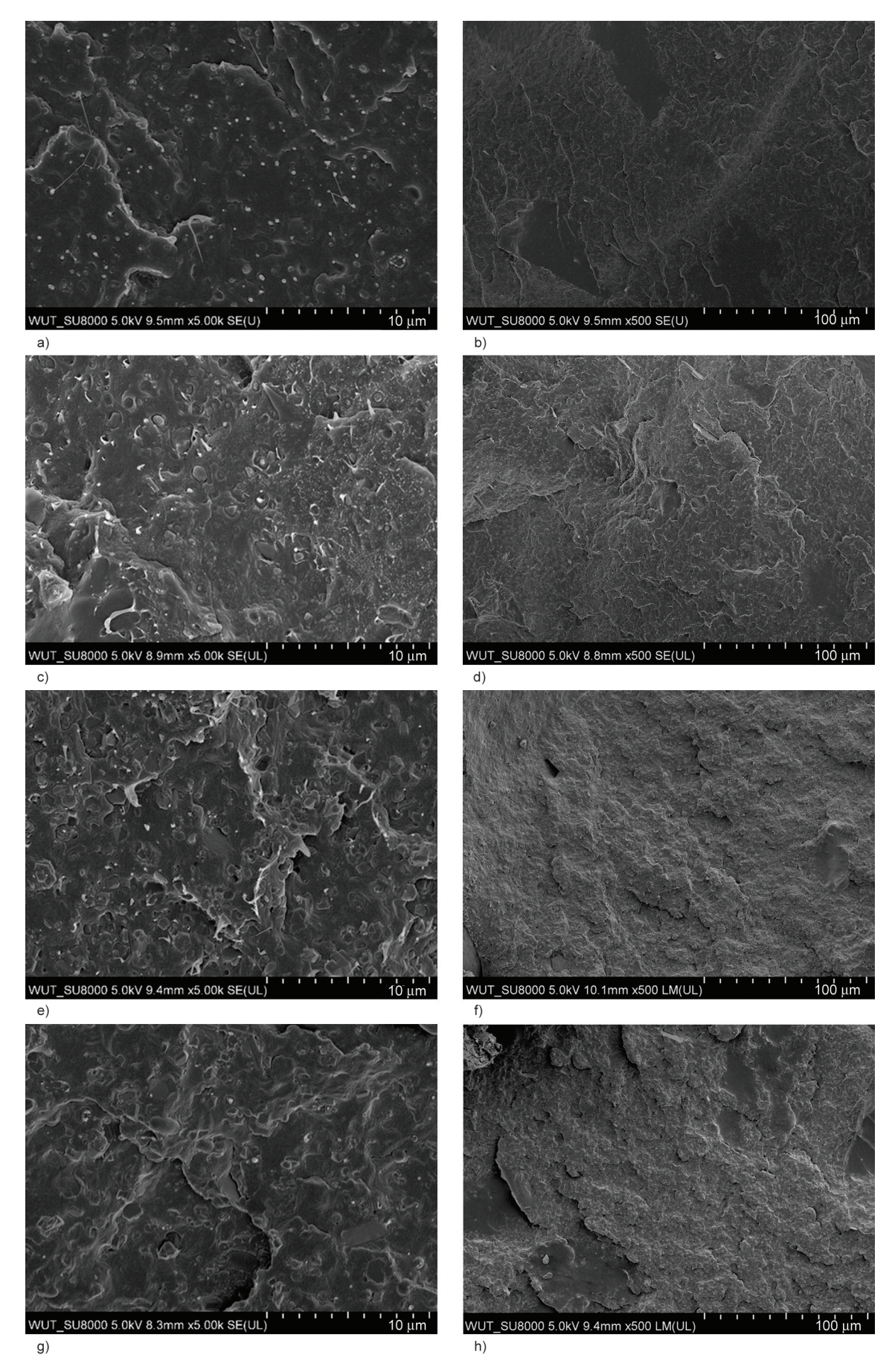


**Figure 2.** SEM images of: a), b) PP70, c), d) 10% ATH-sil, e), f) 20% ATH-sil, g), h) 30% ATH-sil, i), j) 10% MP/AC/PS, k), l) 20% MP/AC/PS, m), n) 30% MP/AC/PS.

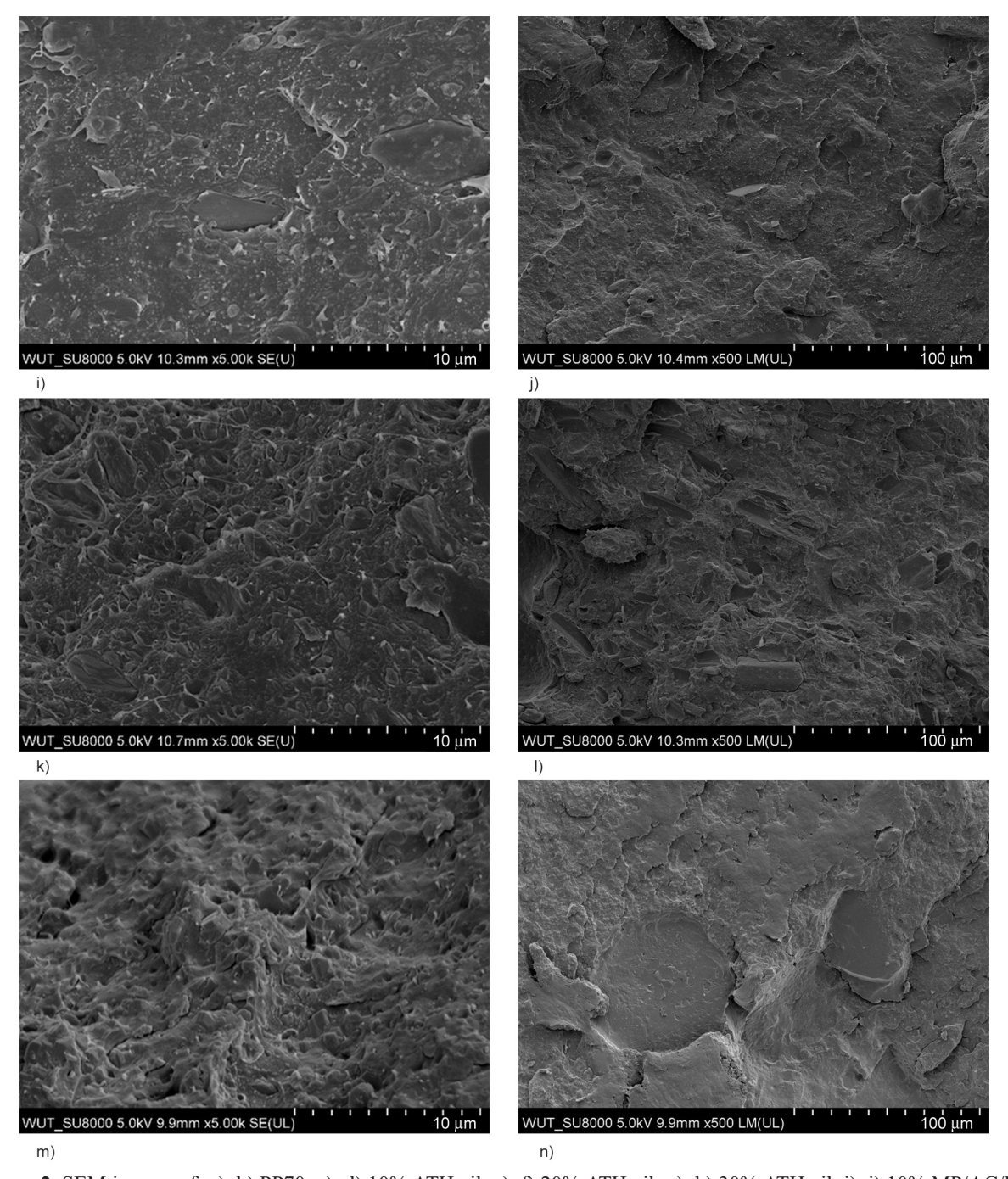


**Figure 2.** SEM images of: a), b) PP70, c), d) 10% ATH-sil, e), f) 20% ATH-sil, g), h) 30% ATH-sil, i), j) 10% MP/AC/PS, k), l) 20% MP/AC/PS, m), n) 30% MP/AC/PS.

to the observed decrease in crystallinity. The results reported by Lima *et al.* [55] indicate a nucleating effect of ground tire rubber on PP, with a simultaneous phenomenon of interfering with the growth of the crystallites, which reduces their greater dimension and higher dispersion reflected in limited  $\Delta H_{\rm m}$  and  $T_{\rm m}$  in comparison to pure PP reported values [38, 56, 57]. At the same time, it should be remembered that PE is immiscible with PP [58] and that the rubber-originated filler additive does not significantly affect the polyethylene crystallinity [59]. The melting

enthalpy comparable for all systems may indicate an additional nucleating effect of non-soluble in the polymeric matrix and processing temperature-stable FRs, which may concern both the dominant fraction of PP [60] and the small amount of HDPE [61]. The retention of a similar  $\Delta H_{\rm m}$  value with decreasing polymer content concerning internal additives, showing thermal effects accompanying the phase transition, indicates this type of interaction. In summary, from the application point of view, the results obtained allow us to conclude that there is a lack of

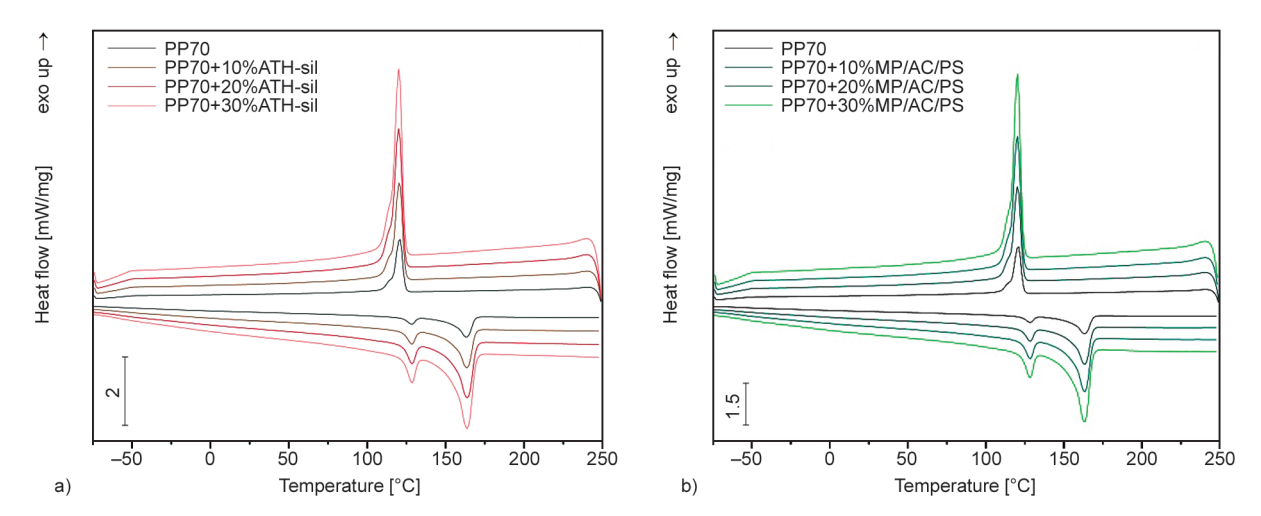


**Figure 3.** DSC thermograms recorded during 2<sup>nd</sup> heating and cooling of PP70-based compositions containing two systems of flame retardants. a) ATH-sil, b) MP/AC/PS.

**Table 2.** Thermal properties determined from DSC.

Sample	T <sub>m</sub> [°C]	$\Delta H_{ m m}$ [J/g]	<i>T</i> <sub>c</sub> [°C]	$\Delta H_{ m c}$ [J/g]	X <sub>c</sub> [%]
PP70	163.2	70.9	120.7	64.9	55.2
PP70+10%ATH-sil	163.8	69.8	120.1	59.3	49.8
PP70+20%ATH-sil	164.6	69.5	119.6	63.2	44.5
PP70+30%ATH-sil	163.6	70.5	120.3	60.4	38.7
PP70+10%MP/AC/PS	163.4	72.9	119.9	67.6	49.7
PP70+20%MP/AC/PS	163.3	71.1	119.6	66.5	44.2
PP70+30%MP/AC/PS	162.8	70.6	120.2	65.1	38.5

 $T_{\rm m},\,\Delta H_{\rm m}-\,$  melting temperature and the corresponding enthalpy of melting

adverse effects induced by both FR systems. Their introduction, even in large quantities, should not necessitate extending the cooling cycle during melt processing.

# 3.3. Thermomechanical properties

The results of the HDT/Vicat test (Figure 4) partly reflected the changes recorded during the DMA analysis. As can be easily predicted, the lowest values of both factors were observed for the unmodified PP70 compound, 57 and 45 °C for the Vicat and HDT tests, respectively. Similar to the results of the DMA analysis, it is evident that the observed changes are not significant, considering the potential changes that might be observed in PP-based materials. The highest thermal resistance for 30% loaded samples ranged from 65 to 70 °C, while other studies indicate that for polypropylene, it is possible to obtain the HDT results of more than 150 °C [62, 63]. However, in most cases, the PP matrix was reinforced with fibrous fillers or prepared with the addition of nucleating

agents, whereas for the developed materials, the additive system consisted of powder-type fillers. The reinforcing efficiency of the spherical type of additives is much less favorable than micro/nano fibers [64–66]. Additionally, for the presented study, the main matrix compound (PP70) contains 30% of the soft rubber phase, whose participation in the structure makes it difficult to increase thermomechanical stability [67, 68]. Nevertheless, for samples containing 30% of the MP/AC/PS fire-retardant system, the HDT result of 70 °C indicates some more visible improvement, which might suggest that, compared to ATH-sil, the prepared mixture leads to a more effective reinforcing mechanism, unlike amorphous materials, where thermal resistance is strongly connected to the glass transition region of the matrix polymer [69, 70], while for semi-crystalline PP, the thermal resistance temperature is a multifactorial phenomenon. In most cases, the significant improvement in thermomechanical properties of PP-based compositions results from the combination of the reinforcement

 $T_{\rm c}, \Delta H_{\rm c}$  – crystallization temperature and the corresponding enthalpy of crystallization

 $X_{\rm c}$  – degree of crystallinity

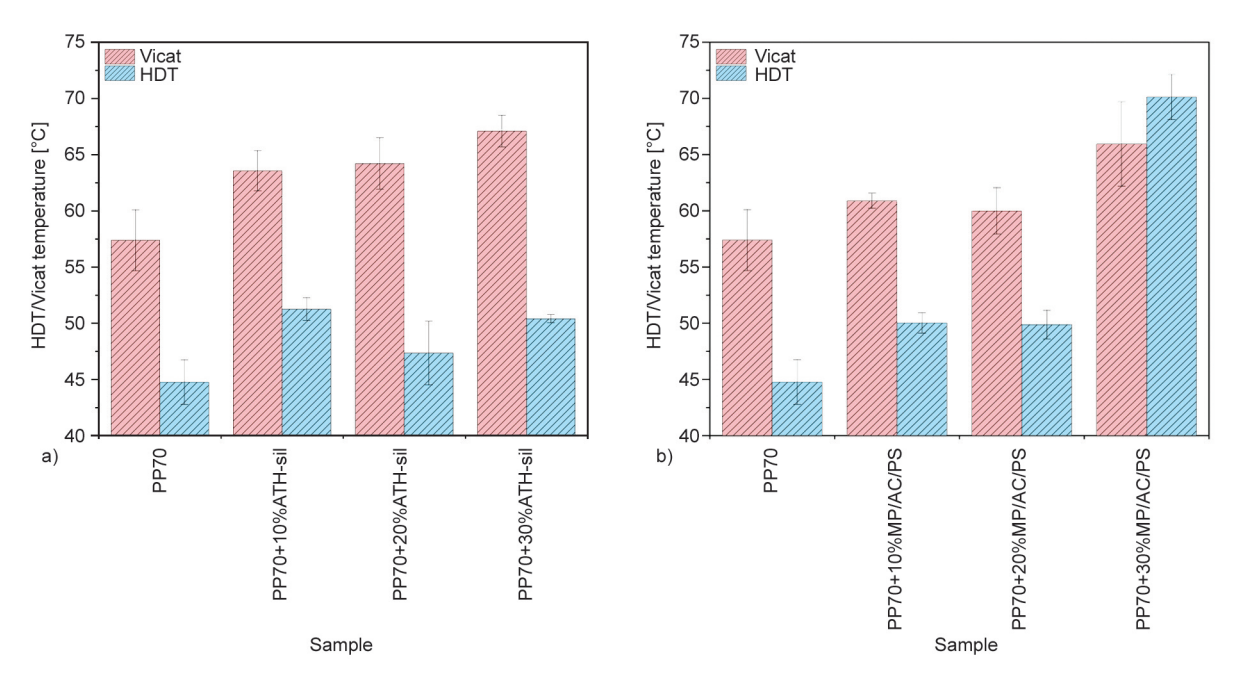


**Figure 4.** The results of the HDT/Vicat temperature measurements for: a) ATH-sil modified materials; b) MP/AC/PS system-based samples.

efficiency of the used fillers and changes that take place in the crystalline structure morphology [71, 72]. For the discussed case, the reinforcing efficiency of ATH-sil might be less effective; however, due to the fact that the clearly better HDT results for the MP/AC/PS additives are still far worse than many available PP-based materials, it is difficult to point out the specific factor that determines the observed improvement in the thermal resistance.

Figure 5 shows thermomechanical curves representing the change of storage modulus (G') and damping factor  $(\tan \delta)$  as a function of temperature. Additional information about storage modulus values at characteristic temperatures (-80, -20, 0, 20, and 80 °C), relaxation temperatures with corresponding tanδ values, and the effectiveness of the filler 'C' calculated according to Equation (1) are collectively presented in Table 3. The introduction of FR caused an increase in the storage modulus of the modified materials compared to PP70 in the entire analyzed temperature range. Increasing the amount of FR gradually increased G' for both series; however, the highest FR con-centration (30 wt%), the ATH-sil series, exhibited more pronounced G' values. Considering the relationship reported in the literature between the elastic modulus determined in the quasi-static tensile test and the storage modulus determined by DMA [73], the results of both tests are also correlated in the considered case. The FR-induced increase in the stiffness of materials at elevat-ed temperatures observed in the thermomechanical evaluation conducted by VST and HDT, was also in line with the thermomechanical properties determined under dynamic conditions.

For both considered material series (ATH and MP/AP/PS-filled), three relaxation temperatures are observed on the  $\tan \delta vs.$  (T) curves: -70 to -20, -20 to 20, and 60–100 °C. The distinguished peak in the lowest temperature range corresponds to the relaxation of the ground elastomer used as a filler [74]; the following maximum at about 0 °C is related to the β-relaxation of polypropylene interpreted as relaxation within the amorphous phase, and the observed  $\alpha$ -relaxation in the highest of the temperatures mentioned above ranges with a maximum at about 80 °C is related to complex changes coinciding in crystals and adducted disordered regions [75]. In all series, the relaxation temperature originating from the elastomer fraction remained unchanged, indicating that the flame-retardant addition had no influence on the elastomer's interactions and dispersions within the polypropylene matrix. However, changes in the TEL relaxation range and the change in the FR share are observed. It cannot be excluded that an additional influence on the changes in relaxation originating from the elastomer may have the  $\gamma$ -relaxation of polypropylene, usually occurring at about -40 °C, overlapping in this case, originating from sub-segmental and side chain relaxations [75, 76]. In the temperature range considered, potentially visible

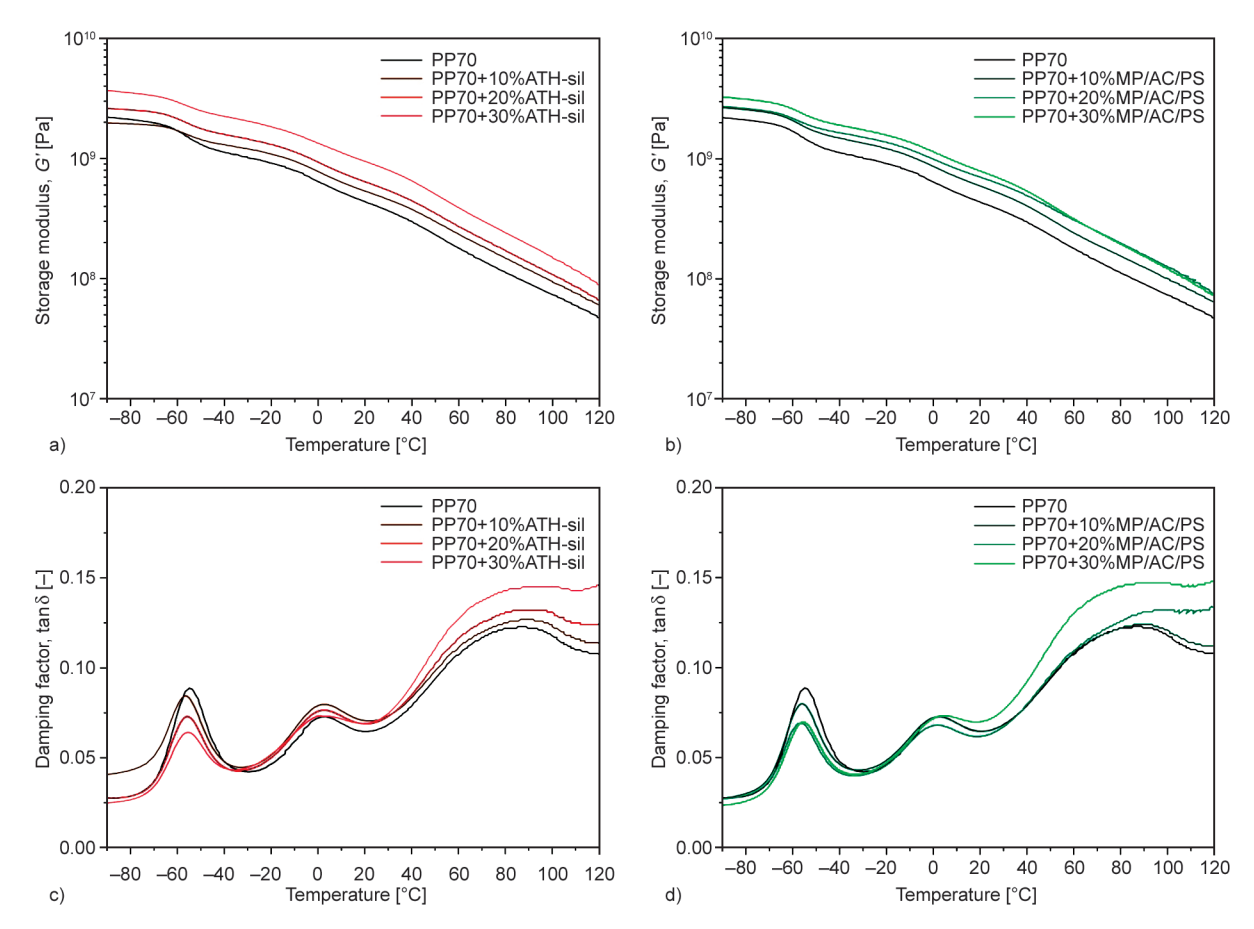


**Figure 5.** a), b) Storage modulus and c), d) damping factor *vs.* temperature curves of polypropylene compositions with various content of FR.

Table 3. Thermomechanical parameters of polypropylene compositions with various content of FR.

Sample	<i>G</i> ′ <sub>-80 °C</sub> [Pa]	<i>G</i> ′ <sub>−20 °C</sub> [Pa]	<i>G</i> ′ <sub>0°C</sub> [Pa]	<i>G</i> ′ <sub>20°C</sub> [Pa]	<i>G</i> ′ <sub>80 °C</sub> [Pa]	<i>T</i> <sub>EL</sub> [°C; −]	$T_{eta ext{PPP}} \ [^{\circ} ext{C};-]$	<i>T</i> <sub>αPP</sub> [°C; –]	<i>C</i> [-]
PP70	$6.04 \cdot 10^9$	9.12·10 <sup>8</sup>	6.46·10 <sup>8</sup>	4.39·10 <sup>8</sup>	1.12·10 <sup>8</sup>	-54.9; 0.088	3.24; 0.073	87.3; 0.123	_
PP70+10%ATH sil	1.94·10 <sup>9</sup>	1.09·10 <sup>9</sup>	$7.74 \cdot 10^8$	5.36·10 <sup>8</sup>	1.47·108	-56.6; 0.084	2.58; 0.080	89.6; 0.127	0.700
PP70+20%ATH-sil	$2.54 \cdot 10^9$	1.31.109	$9.27 \cdot 10^8$	6.41.108	$1.70 \cdot 10^8$	-55.9; 0.073	2.56; 0.076	90.4; 0.132	0.793
PP70+30%ATH-sil	3.53·10 <sup>9</sup>	1.85·10 <sup>9</sup>	$1.33 \cdot 10^9$	9.46·10 <sup>8</sup>	$2.40 \cdot 10^8$	-55.9; 0.064	3.50; 0.073	95.2; 0.145	0.781
PP70+10%MP/AP/PS	$2.57 \cdot 10^9$	1.22·10 <sup>9</sup>	$8.61 \cdot 10^{8}$	5.96·10 <sup>8</sup>	$1.55 \cdot 10^8$	-55.9; 0.080	2.57; 0.073	89.6; 0.124	0.880
PP70+20%MP/AP/PS	$2.62 \cdot 10^9$	1.38·10 <sup>9</sup>	$9.90 \cdot 10^{8}$	$7.07 \cdot 10^8$	1.99·10 <sup>8</sup>	-56.7; 0.069	1.80; 0.068	98.2; 0.132	0.699
PP70+30%MP/AP/PS	$3.14 \cdot 10^9$	$1.58 \cdot 10^9$	$1.14 \cdot 10^9$	$7.94 \cdot 10^8$	$1.94 \cdot 10^8$	-55.1; 0.070	4.24; 0.073	95.0; 0.147	0.859

 $G'_{\text{x}^{\circ}\text{C}}$  – storage modulus estimated in selected temperatures (-80, -20, 0, 20, and 80 °C)  $T_{\text{EL}}$ ,  $T_{\alpha\text{PP}}$ ,  $T_{\beta\text{PP}}$  – temperatures corresponding to elastomeric filler, and PP  $\alpha$ -,  $\beta$ -relaxations C – factor calculated according to Equation (1)

maxima on the  $\tan \delta(T)$  curves resulting from HDPE, present in the polymeric matrix structure, corresponding to β-relaxation, occur at about  $-20\,^{\circ}\mathrm{C}$  [77]. Due to the overlapping effects originating from the dominant share of PP and other components, a small concentration of polyethylene did not significantly affect the course of the DMA curves, *i.e.*, additional peaks at damping factor vs. temperature curves. The presence of HDPE can be attributed to the continuation of the rising trend in the DMA curve after reaching

 $\alpha$ -relaxation originating from polypropylene above 100 °C and corresponds to the beginning of the melting of the HDPE fraction.

The increase in the  $\alpha$ -relaxation temperature of PP with rising FR share in material can be related to two different phenomena: (i) increased amount of crystalline phase caused by nucleating ability on PP of ATH [78] and PS [79] translating into a more significant number of crystalline domains increasing the energy necessary for the relaxation process, and/or

(ii) significant interphase interactions between the components of the composition, as confirmed by simultane-ous increase of G' and  $T_{\alpha PP}$ . The dominant share of the first of the phenomena mentioned above in the impact on the PP matrix may confirm the lack of significant dependence in the temperature range corresponding to the relaxation of the amorphous domains of the polymer matrix  $(T_{\beta PP})$ .

Determination of the C-factor can be a valuable tool for qualitative comparative evaluation of the thermomechanical properties of materials, considering the change in interphase inter-actions within the system [80, 81]. The interpretation assumes that the lower the C value, the more intensive the effectiveness of the dispersed phase's interaction with the polymer matrix. It can be observed that the greater effectiveness of the ATH filler's interaction can be related to a more favorable dispersion in comparison to the ternary MP/AP/PS system. Lower C values for all series of the single-component FR system can also be related to increased adhesion to the non-polar polymer matrix resulting from silanization.

#### 3.4. Mechanical and processing properties

The incorporation of all additives into the semi-crystalline polymer matrix, even in low amounts, can affect the material's mechanical properties directly by the addition itself and indirectly by affecting its processing and thus resulting in structural properties [82]. Therefore, the effect of the incorporation of two flame-retardant systems simultaneously filled with tire rubber crumbs was investigated. The representative stress-strain curves are presented in Figure 6. Table 4 summarizes the data obtained from melt flow measurement, Shore D hardness, static tensile, and rebound resilience tests. It was found that, along with

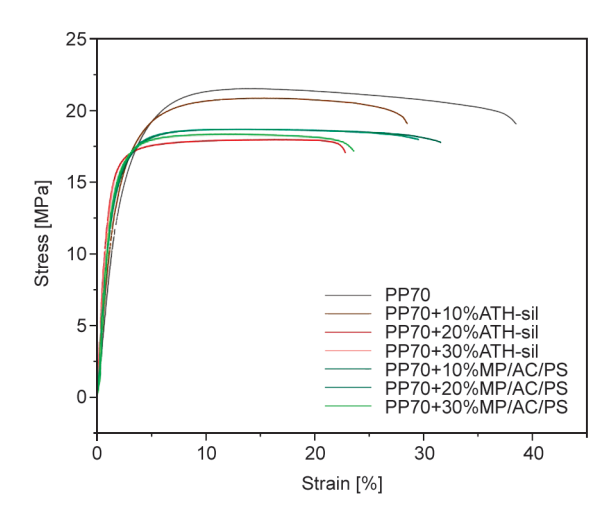


**Figure 6.** Representative stress-strain curves of the prepared materials

the incorporation of flame retardants, a decrease in the MFR was observed. A much more intense impact on the MFR value was observed for the MP/AC/PS system. This might result from the interfacial interactions between the additive and the polymer, which can hinder the mobility of polymer chains, making it more difficult for the polymer to flow and reducing the melt flow rate.

Considering the mechanical properties changes induced by the incorporation of FRs into the PP70, a stiffening nature of the addition of modifiers was observed, which is reflected in the increase in the value of Young's modulus (*E*) and decrease in elongation at break. The most intense increase in *E* was observed for the system containing 30% ATH-sil and was almost two-fold higher than for the reference sample. The elongation at break values were also significantly reduced for the composition comprising the highest amount of flame retardants (30%). Moreover, the tensile strength mean values decreased

Table 4. Melt flow rate and mechanical properties of the series of PP70-based compositions containing flame retardants.

Material	MFR [g/10 min]	E [MPa])	Tensile strength [MPa]	ε <sub>b</sub> [%]	Shore D hardness	<i>RR</i> [%]
PP70	6.7±0.3	615.1±98.1	21.4±0.4	35.7±3.3	67.8±0.9	30.9±1.1
PP70+10%ATH-sil	5.3±0.2	825.4±128.2	20.7±0.3	31.6±5.6	67.0±0.5	30.0±1.2
PP70+20%ATH-sil	5.1±0.2	1031.1±141.1	17.6±0.7	21.2±3.7	67.9±0.6	29.0±1.1
PP70+30%ATH-sil	4.2±0.1	1290.2±198.3	17.4±0.2	18.4±1.3	67.9±0.7	26.0±1.0
PP70+10%MP/AC/PS	4.8±0.1	649.3±178.4	20.7±0.4	31.8±0.9	67.1±1.0	29.6±1.1
PP70+20%MP/AC/PS	4.3±0.6	931.1±112.5	18.7±0.8	31.1±1.1	67.0±0.8	27.0±1.5
PP70+30%MP/AC/PS	3.47±0.3	950.1±147.1	17.9±1.3	21.5±2.7	69.0±0.9	22.6±2.0

MFR - melt flow rate

E – Young's modulus

 $\varepsilon_b$  – elongation at break

RR - rebound resilience

slightly with the increase in the amount of flame retardants in the system. While no significant improvement in mechanical properties was initially expected for the MP/AC/PS mixture, an increase in Young's modulus was in fact observed. In contrast, for the system with ATH-sil, a more pronounced improvement was anticipated. Silane coupling agents are commonly used in mineral- and glass-filled composites to enhance mechanical performance and durability by strengthening the interface and minimizing property loss, often caused by mois-ture exposure. Recent studies have developed advanced silane systems to achieve stronger and more stable bonds [83]. However, in this work, the expected improvement in mechanical proper-ties with ATH-sil was not clearly evident. This can be attributed to the specific nature of the PP70 system, which combines PP with recycled tire rubber crumbs. This Trc is generally composed of a complex mixture of polymers, fillers, and additives, predominantly based on styrene-butadiene rubber (SBR) and natural rubber, but often with some nitrile butadiene rubber (NBR) components. These elastomeric phases present a highly crosslinked and chemically heterogeneous structure, which limits the accessibility and reactivity of silane coupling agents at the rubber surface. Silane coupling agents generally show a stronger affinity toward polar or hydroxyl-containing surfaces due to their ability to form siloxane or hydrogen bonds [83]. ATH particles provide hydroxyl groups that can react with silanes, promoting good bonding with more polar phases. However, PP is a nonpolar polyolefin with very low surface energy and lacks functional groups for silane reactivity. Therefore, the silane coupling of ATH tends to be more effective with polar elastomeric domains, such as NBR fragments, rather than the PP matrix. In our case, the recycled Trc presents a mostly saturated, crosslinked network, reducing the availability of reactive sites, which may explain the limited compatibilization and mechanical reinforcement observed.

The choice of the hardness measurement method was guided by the possibility of comparison with the elastomeric material used as a filler. The experimental results showed that the effect of the presence of an additional 30 wt% of FRs can be omitted.

The ability to rebound quickly can be treated as an indication related to assessing materials' shock-absorbing and dynamic properties. It is assumed that when considering rebound applications, resilience

values of 10-20% are characteristic of shock-absorbing materials and between 40 and 70% for applications that demand quick recovery [84]. The obtained RR values for polypropylene containing 30 wt% of tire rubber crumbs at ~30% align with the similar results presented by Raue and Ehrenstein for PP/styrene ethylene propylene styrene (SEPS) compounds [85]. Introducing fillers in dispersed and insoluble polymeric matrix inclusions gradually decreased RR with the increasing share of FRs, a previously described effect [86]. A more pronounced effect was noted for systems containing a mixture of MP/AC/PS. Taking into account the negligible impact of the addition of FRs on the hardness of the materials and the increased stiffness of the modified series, it can be concluded that the more significant influence on the RR results may be related to better dispersion of multicomponent series and the complex interfacial structure of the material, which was treated as a highly-filled composite.

### 3.5. Thermal stability and gas analysis

Thermogravimetric analysis, performed in nitrogen, evaluated the thermal stability of the investigated materials. Additionally, analyses in air determined the residue yield in the presence of oxygen. Figure 7 displays the curves of mass and derivatives as a temperature function (DTG), while the obtained data are summarized in Table 5.

The polymer's onset degradation temperature, corresponding to 5% weight loss, was 345°C, while for samples with flame retardants, a decrease resulting from their mode of action was noted. The maximal reduction was observed for PP70+30%ATH and achieved 46 °C. The most intense degradation step, related to the polymer's decomposition, appeared at 460 °C. Due to the complex structure of the elastomer, DTG presents an additional stage, at approx. 380 °C. The first peak corresponds to the rubber degradation [87], while the second one is attributed to the PP matrix. These temperatures are kept relatively unchanged, but the incorporation of ATH leads to the appearance of the third step at about 300 °C, related to ATH degradation by the release of water molecules, which leads to the production of alumina [88].

For the proposed green FR system, additional steps corresponding to the degradation of components, such as hemicellulose, lignin, and cellulose occurring at 250–290, 350–390, and 190–450 °C, respectively, can be observed. Melamine phosphate decomposes

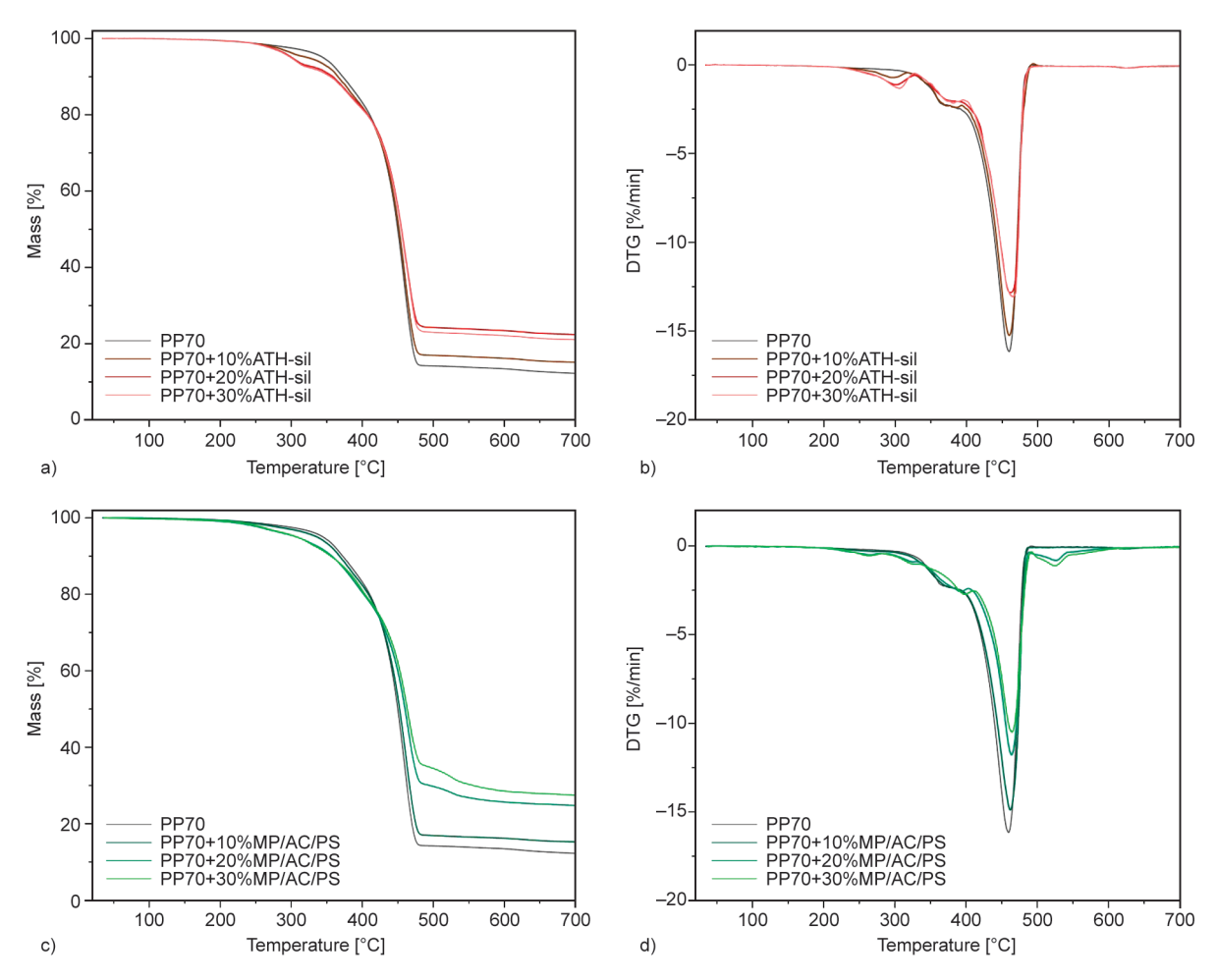


Figure 7. TGA results for PP70 with FR systems; a), c) mass and b), d) DTG curves.

**Table 5.** The results from the TGA.

Sample	T <sub>5%</sub> [°C]	DTG <sub>1</sub> [°C; %/min]	DTG <sub>2</sub> [°C; %/min]	DTG <sub>3</sub> [°C; %/min]	DTG <sub>4</sub> [°C; %/min]	DTG <sub>5</sub> [°C; %/min]	Residue at 900°C in nitrogen [%]	Residue at 900°C in air [%]
PP70	345	_	_	383; 0.24	459; 1.60	_	10.7	5.0
PP70+10%ATH-sil	323	299; 0.07	=	382; 0.24	460; 1.53	-	14.3	8.7
PP70+20%ATH-sil	301	305; 0.13	=	380; 0.21	461; 1.27	=	21.5	32.1
PP70+30ATH-sil	299	308; 0.13	=	381; 0.21	462; 1.30	-	20.3	35.4
PP70+10%MP/AC/PS	337	=	=	382; 0.24	463; 1.37	-	14.4	6.2
PP70+20%MP/AC/PS	307	265; 0.05	327; 0.09	391; 0.25	463; 0.17	524; 0.08	23.7	21.8
PP70+30%MP/AC/PS	308	263; 0.05	330; 0.10	399; 0.27	465; 1.00	525; 0.11	25.7	22.8

 $T_{5\%}$  – temperatures corresponding to 5% weight loss;

 $DTG_x$  – temperature corresponding to the maximum of mass loss.

at 240 °C, leaving a high amount of residual char [28]. Furthermore, a secondary peak over 520 °C appears, re-lated to the formation of transient char. Applying a multi-component FR system led to peaks shifting temperatures and their overlap. The change in decomposition rates in each stage led to a higher residue than PP70, regardless of the oxygen access. As a result, the residue yield increased from 10 to 25% for PP70+MP/AC/PS for analyses conducted

under anaerobic conditions and 35% for PP70+30%ATH-sil in air. The change in the materials' thermal stability causes degradation at earlier temperatures, although still at higher values than the ones used during processing, thus ensuring the material is processable by conventional forming processes without degradation.

The analysis of the evolved gases from the TG assessment via FTIR spectroscopy revealed a similar

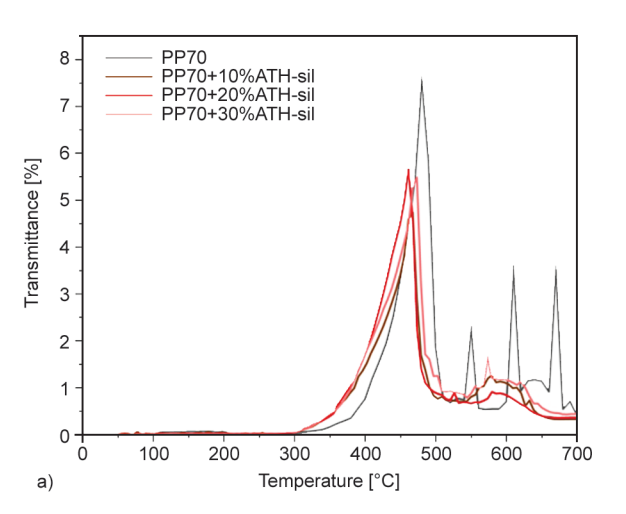
degradation process regardless of the share or type of FR used. Figure 8 shows the Gram-Schmidt profile for the different samples, giving a representation of the moments where relevant spectra are collected. It is found that for unmodified PP, four peaks appear at 470, 540, 600 and 660 °C, and the most significant signal is obtained at 470 °C, which is related to the degradation of PP as a major component.

When analyzing the spectrum collected within the temperature range studied (Figure 9), basically two main distinct steps can be identified, *i.e.* the release of alkanes and olefins derived from PP (between 3080 and 2900 cm<sup>-1</sup> mainly, also observed at 1400 to 1650 cm<sup>-1</sup>) [89]. Some weak absorption bands start to appear and intensify with increased temperatures, particularly around 1700–1800 cm<sup>-1</sup>, related to the oxidation of PP (C=O) [28]. After a certain moment, close to 500 C, the bands attributed to alkanes disappear. From that moment, other absorption bands appear, in the range about 2200–2300, 1300–1500

and 700–900 cm<sup>-1</sup> can be found. In particular, these bands correspond to the formation of CO<sub>2</sub> (2400–2200 and 700–900 cm<sup>-1</sup>) [90, 91], while the peak at 1300–1500 cm<sup>-1</sup> can be related to the appearance of methyl bending in alkenes and the one at about 700 cm<sup>-1</sup> (C–H in aromatic groups) [91, 92]. It can be clearly observed that the spectra for the three series of materials are practically the same. For those at lower temperature (Figure 9a), the main differences are observed in the range of 2000–2400 cm<sup>-1</sup>, where some weak bands are visible, particularly for the samples with ATH, attributed to the formation of CO<sub>2</sub>. This is correlated to the higher relative absorbance of the peak at 1722 cm<sup>-1</sup>, attributed to the oxidation of PP.

#### 3.6. Flammability assessment

The UL 94 flame test is designed to compare the flammability of various materials, especially those used in electrotechnical and automotive applications.



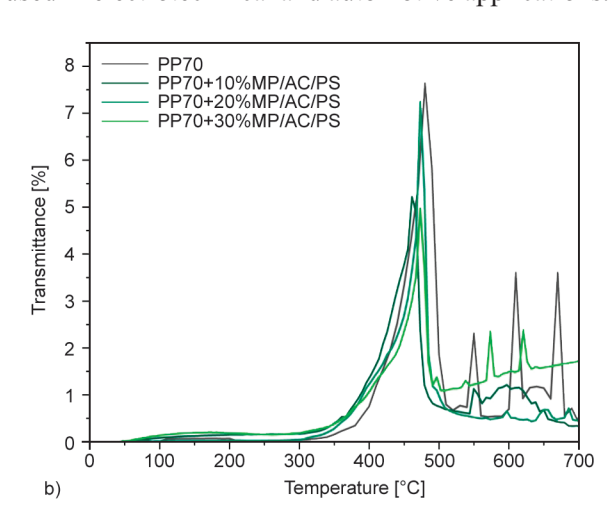
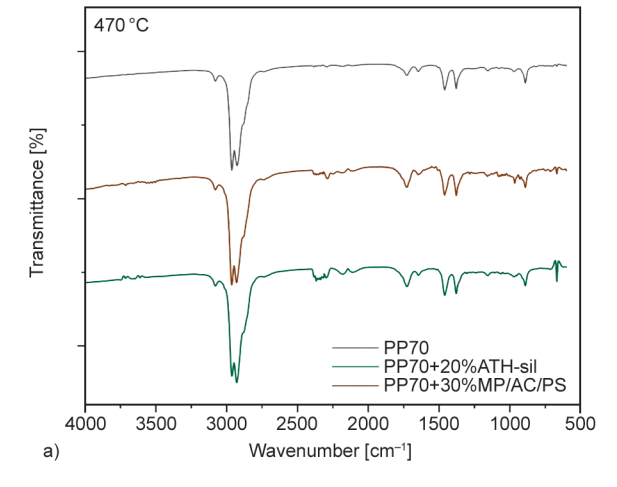
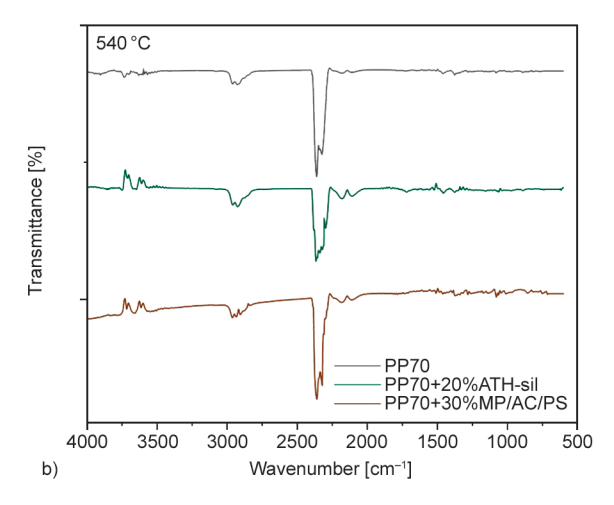


Figure 8. Gram-Schmidt profiles for the compositions containing a) ATH-sil and b) MP/AC/PS.





**Figure 9.** Spectra for evolved gases at a) 470 °C and b) 540 °C, for the series PP70, PP70+30%ATH-sil, and PP70+30%MP/AC/PS.

<b>Table 6.</b> Flammability	testing of samples	s via UL 94	1 investi-
gations.			

Sample	Bı [	Class		
PP70	43	43	43	HB40
PP70+10%ATH-sil	33	35	33	HB
PP70+20%ATH-sil	30	20	24	HB
PP70+30%ATH-sil	17	16	18	HB
PP70+10%MP/AP/PS	43	40	45	HB40
PP70+20%MP/AP/PS	37	37	29	HB
PP70+30%MP/AP/PS	28	25	27	НВ

Vertically or horizontally arranged samples are exposed to a small ignition source with a nominal thermal output of 50 W. These test methods are used to determine the linear burning rate or the self-extinguishing properties of the polymer. The UL 94 results of horizontally orientated samples are presented in Table 6.

Since prolonged burning, supported by char formation, resulted in the clamp being reached by flame, all tested materials in the case of the vertical method were out of class. Therefore, their results were not presented in the table, and a horizontal test was performed. PP70 without flame retardants, as well as 10%MP/AP/PS, were classified as HB40 class, while the rest of the samples as HB class due to their linear burning rate below 40 mm/min. The addition of the flame retardants significantly reduced the flame speed, especially in the case of the ATH-sil series. For both the ATH-sil and MP/AC/PS series, the linear burning rate decreased with increasing flame retardant amount, reaching the lowest values for 30 wt%. The impact of developed flame-retardant systems on the polymers' burning behavior was assessed via cone calorimetry tests. The heat release curves (HRR), photographs of residue, and data obtained from measurements are presented in Figures 10-12, and Table 7, respectively.

As shown in Figure 10, PP70 exhibited one broad peak with the maximum heat release rate (pHRR) equal to approx. 760 kW/m². Employing ATH-sil resulted in a gradual decrease in the HRR, and the lowest values were achieved for the material with the highest flame-retardant content. ATH extends the time needed for the material to heat up to the ignition temperature, and the release of water vapor reduces the concentration of free radicals and oxygen. Moreover, a layer of Al<sub>2</sub>O<sub>3</sub> is formed on the surface of the polymer, which prevents the heat and oxidant from propagating to deeper layers of the material

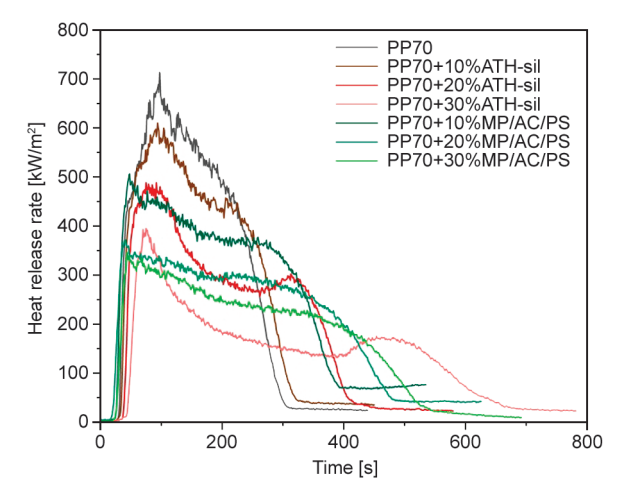


**Figure 10.** Representative heat release rate curves of the investigated materials.

(Figure 10). MP works in both phases, apart from replacing the poly-mer with a less flammable component, increasing the ability of MP to form char. In turn, the structure of PS, rich in polar groups, enhances the effectiveness of phosphorus flame retardant in char formation (Figure 11). The combination of MP, AC, and PS flattened the curves, characteristic of materials able to form a char [93]. The formation of a protective layer is confirmed by the yield of residues that increase with the higher FR content (Table 6) and photographs of the samples after burning (Figure 11). In the case of ATH-sil samples, the residues were compact and had a small thickness. In turn, for the MP+AC+PS series, numerous small holes inside the chars, confirmed by photographs from an optical microscope (Figure 11i), were observed.

The slightly higher values of time to ignition (TTI) were recorded for a series of materials with ATH. which is connected with its mechanism of action described above. In turn, the devel-oped system decreases TTI due to the earlier decomposition of intumescent flame retardant. All used flame retardants led to flammability reduction; however, the lowest pHRR, two times lower than the unmodified polymer, was obtained for PP70+30%MP/AC/PS. Flame retardants also caused a decrease in the maximum average rate of heat emission (MARHE), as one of the indica-tors enabling flame spread evaluation, by 47 and 56% for PP70+30%MP/AC/PS and PP70+30%ATH-sil, respectively. The reduction of total heat release (THR) results from reduced amount of fuel and char formation or incomplete combustion, which occurs due to reduced combustion efficiency, confirmed by lower effective heat of combustion

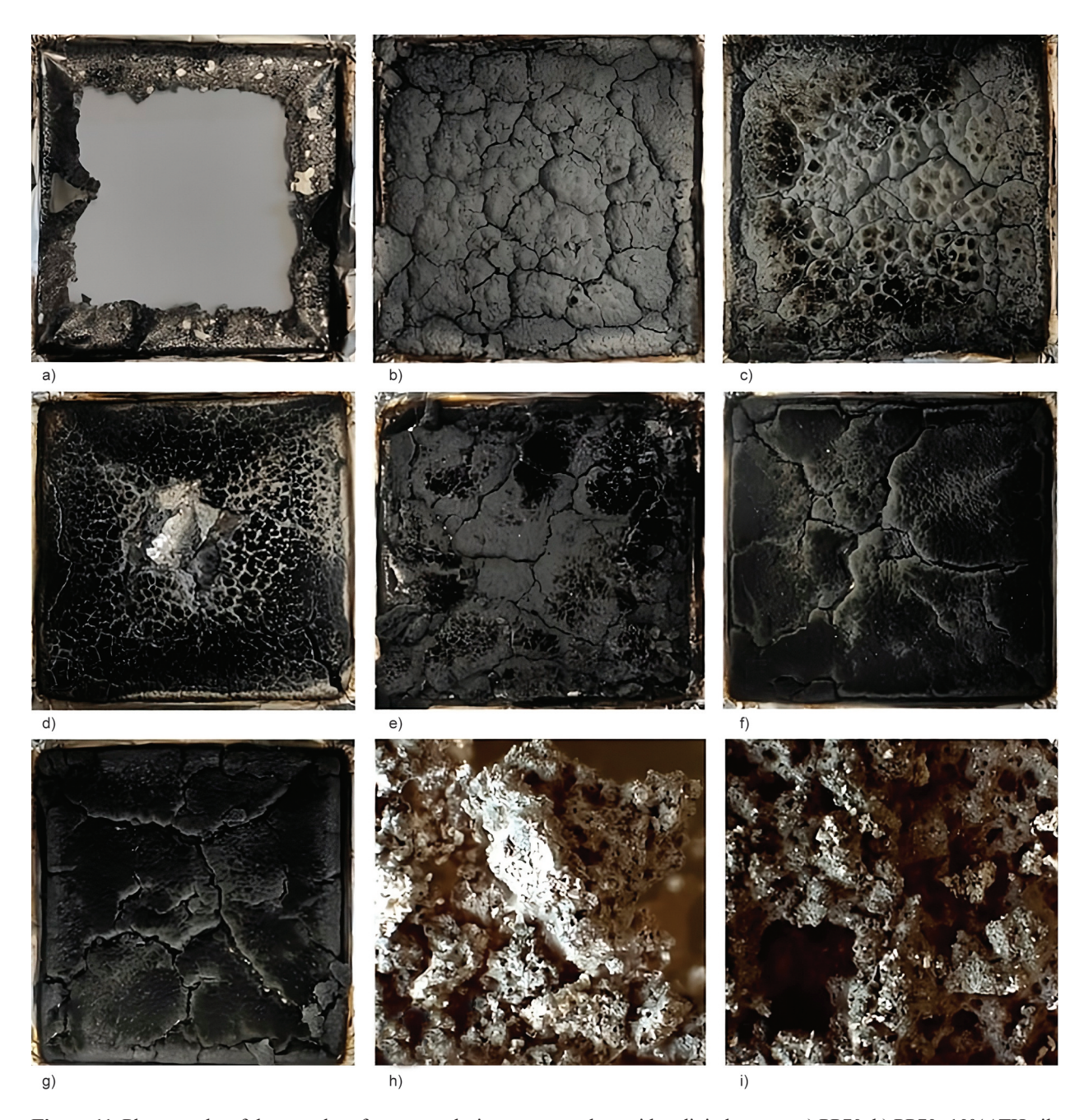


**Figure 11.** Photographs of the samples after cone calorimetry tests taken with a digital camera a) PP70, b) PP70+10%ATH-sil, c) PP70+20%ATH-sil, d) PP70+30%ATH-sil, e) PP70+10%MP/AC/PS, f) PP70+20%MP/AC/PS, g) PP70+30%MP/AC/PS, or optical microscope h) PP70+10%ATH-sil, i) PP70+10%MP/AC/PS.

(EHC) [94]. The lowest val-ues for both THR and EHC were observed for PP with 30% of ATH-sil. The use of large amounts of this flame retardant also resulted in the most significant reduction in smoke emissions, assessed based on total smoke release (TSR), which results from the dilution of the gas phase. It should be noted that although ATH showed the best effectiveness in reducing burning and smoke emissions, the effect was achieved only when its share was 30% by mass. A significant increase in efficiency, due to the increase in the share of ATH-sil

from 20 to 30 wt%, also confirmed the course of the TSR curves (Figure 12).

#### 4. Conclusions

Two series of post-consumer PP with 30 wt% of tire rubber crumbs containing 10, 20, and 30 wt% of two flame retardant systems have been prepared using a twin-screw extruder. The structure and composition of the analyzed systems were investigated utilizing FTIR spectroscopy. In the case of ATH-sil containing compositions, one observed characteristic absorption

**Table 7.** Cone calorimeter results for polymers with fire retardant systems.

Materials	TTI [s]	pHRR [kW/m²]	MARHE [kW/m²]	THR [MJ/m²]	EHC [MJ/kg]	TSR [m²/m²]	Residue [%]
PP70	37±2	756±87	472±12	124±1	39±0	2218±115	11±0
PP70+10%ATH-sil	39±2	602±29	409±20	122±1	38±0	2148±46	15±0
PP70+20%ATH-sil	42±1	493±22	311±10	116±2	36±1	1979±98	21±0
PP70+30%ATH-sil	45±2	398±12	209±6	106±2	34±1	1535±52	30±1
PP70+10%MP/AC/PS	30±3	502±27	359±26	126±10	39±3	2168±154	13±0
PP70+20%MP/AC/PS	27±2	371±4	269±12	120±5	37±2	1801±120	21±0
PP70+30%MP/AC/PS	31±1	344±12	249±14	120±20	37±4	1841±108	26±4

TTI - time of ignition

pHRR - peak of heat release rate

MARHE - maximum average rate of heat emission

THR - total heat release

EHC - effective heat of combustion

TSR - total smoke release

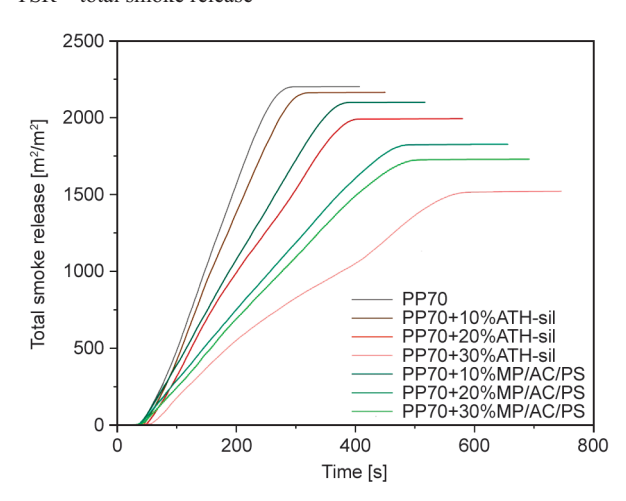


**Figure 12.** Representative total smoke release curves of both series.

bands at 661 and 963 cm<sup>-1</sup> related to the Al-O stretching vibrations, as well as the stretching NH<sub>2</sub> vibra-tion at 3452 cm<sup>-1</sup>, which were due to surface modification by the silane coupling agent. For the MC/AC/PS series, the main changes are due to the vibration of P-OH in MC and Al-O in AC. In addition, the mechanical properties, hardness, and melt flow rate (MFR) of the compositions have been assessed. DSC studies showed that the addition of these selected systems of flame-retardants caused no effect on the melting and crystallization temperatures of PP70. On the other hand, a reduction of melt flow rate of the compositions is obtained with the increased ratios of both fillers, which also provide a stiffening effect, increasing the elastic modulus and reducing the elongation at break with the same trend. Tensile strength was slightly reduced, particularly

for compositions with over 20 % of the flame retardants, while hardness was not affected by the in-corporation of any of them. This study demonstrates the effective use of different flame-retardant systems in PP/rubber compositions, with a particular focus on ATH-sil and the MP/AC/PS with reduced environmental impact. All tested materials were classified as HB class. Moreover, incorporation of ATH-sil significantly delayed ignition, lowered peak heat release rate (pHRR), and reduced smoke emissions through water release, radical quenching, and the formation of a protective Al<sub>2</sub>O<sub>3</sub> layer. The intumescent MP/AC/PS system promoted char formation, resulting in flattened HRR curves, reduced MARHE, and a twofold decrease in pHRR compared to neat PP. While ATH-sil proved highly effective, its performance was strongly dependent on high loading levels (30 wt%). In contrast, the MP/AC/PS system achieved notable improvements in flame retardancy with enhanced char development and lower heat release parameters.

This work demonstrates, for the first time, how mineral and intumescent systems complement each other in PP/rubber compositions by providing flame inhibition through distinct yet comple-mentary mechanisms in both the gas and condensed phases. These results provide valuable in-sights for designing PP/rubber compositions with tailored flame-retardant systems, balancing efficiency, smoke suppression, and material performance, and demonstrate strategies to meet fire safety requirements in polymer applications.

#### Acknowledgements

The studies were financed by the HORIZON-EIC-2022-ACCELERATION-01 within project no 190108462 (Ecoplastomer). This study was supported by the National Centre for Research and Development of Poland under project LIDER13/0095/2022, Innovative use of lignocellulosic material as a component of the flame-retardant system of polymer products for electrical industry and electromobility. LICEM project (EIS-2021-33), funded by Consejería de Economía, Conocimiento y Empleo, Gobierno de Canarias, through Fondo Europeo de Desarrollo Regional. Canarias Avanza con Europa.

#### References

- [1] Shrivastava A.: Plastic properties and testing. William Andrew, Norwich (2018).
- [2] Geyer R.: Production, use, and fate of synthetic polymers. in 'Plastic waste and recycling' (ed.: Letcher T. M.) Academic Press, Amsterdam, 13–32 (2020). https://doi.org/10.1016/B978-0-12-817880-5.00002-5
- [3] Voet V., Jager J., Folkersma R.: Plastics in the circular economy. de Gruyter, Berlin (2024). https://doi.org/10.1515/9783111201443
- [4] Geyer R., Jambeck J. R., Law K. L.: Production, use, and fate of all plastics ever made. Science Advances, 3, e1700782 (2017). https://doi.org/10.1126/sciadv.1700782
- [5] Winans K., Kendall A., Deng H.: The history and current applications of the circular economy concept. Renewable and Sustainable Energy Reviews, 68, 825–833 (2017).

https://doi.org/10.1016/j.rser.2016.09.123

- [6] Ladhari A., Kucukpinar E., Stoll H., Sängerlaub S.: Comparison of properties with relevance for the automotive sector in mechanically recycled and virgin polypropylene. Recycling, 6, 76 (2021). https://doi.org/10.3390/recycling6040076
- [7] Ignatyev I. A., Thielemans W., Vander Beke B.: Recycling of polymers: A review. ChemSusChem, 7, 1579–1593 (2014).

 $\underline{https:/\!/doi.org/10.1002/cssc.201300898}$ 

- [8] Zambrano C., Tamarit P., Fernandez A. I., Barreneche C.: Recycling of plastics in the automotive sector and methods of removing paint for its revalorization: A critical review. Polymers, 16, 3023 (2024). https://doi.org/10.3390/polym16213023
- [9] Gallone T., Zeni-Guido A.: Closed-loop polypropylene, an opportunity for the automotive sector. Field Actions Science Reports, **19**, 48–53 (2019).
- [10] Jain A. K., Gupta N. K., Singhal R., Nagpal A. K.: Effect of dynamic crosslinking on crystallization and thermal degradation of polypropylene in polypropylene (PP)/ethylene–propylene diene (EPDM) rubber blends. Materials and Manufacturing Processes, 17, 415–431 (2002).

https://doi.org/10.1081/AMP-120005386

- [11] Shafaattalab F., Jalali-Arani A.: Effect of maleic anhydride-grafted polypropylene as a compatibilizer and dynamic vulcanization on morphology, rheology, mechanical and thermal properties of polypropylene/butadiene rubber blend. Journal of Applied Polymer Science, 142, e57006 (2025).
  - https://doi.org/10.1002/app.57006
- [12] Li C., Wang Z., Liu W., Ji X., Su Z.: Copolymer distribution in core–shell rubber particles in high-impact polypropylene investigated by atomic force microscopy–Infrared. Macromolecules, **53**, 2686–2693 (2020). https://doi.org/10.1021/acs.macromol.0c00328
- [13] Paszkiewicz S., Andrzejewski J., Grochała D., Adamczyk K., Figiel P., Piesowicz E., Pokwicka-Croucher K.: Thinking green on 3D printing: Sustainable polymer compositions of post-consumer polypropylene and tire rubber crumbs intended for industrial applications. Materials, 17, 5209 (2024). https://doi.org/10.3390/ma17215209
- [14] Martey S., Hendren K., Farfaras N., Kelly J. C., Newsome M., Ciesielska-Wrobel I., Sobkowicz M. J., Chen W-T.: Recycling of pretreated polyolefin-based ocean-bound plastic waste by incorporating clay and rubber. Recycling, 7, 25 (2022). https://doi.org/10.3390/recycling7020025
- [15] Cullis F. C., Hirschter M. C.: The combustion of organic polymers. Clarendon Press, Oxford (1981).
- [16] Camino G., Costa L., Luda di Cortemiglia M. P.: Overview of fire retardant mechanisms. Polymer Degradation and Stability, 33, 131–154 (1991). https://doi.org/10.1016/0141-3910(91)90014-I
- [17] Idumah C. I., Hassan A., Affam A. C.: A review of recent developments in flammability of polymer nanocomposites. Reviews in Chemical Engineering, 31, 149–177 (2015). https://doi.org/10.1515/revce-2014-0038
- [18] Lyon R. E., Walters R. N.: Flammability of automotive plastics. in 'SAE World Congress and Exposition, Detroit, USA' 1–17 (2006). <a href="https://doi.org/10.4271/2006-01-1010">https://doi.org/10.4271/2006-01-1010</a>
- [19] Seidi F., Movahedifar E., Naderi G., Akbari V., Ducos F., Shamsi R., Vahabi H., Saeb M. R.: Flame retardant polypropylenes: A review. Polymers, 12, 1701 (2020). https://doi.org/10.3390/polym12081701
- [20] Wang C., Cai L., Shi S. Q., Wang G., Cheng H., Zhang S.: Thermal and flammable properties of bamboo pulp fiber/high-density polyethylene composites: Influence of preparation technology, nano calcium carbonate and fiber content. Renewable Energy, 134, 436–445 (2019). https://doi.org/10.1016/j.renene.2018.09.051
- [21] van der Veen I., de Boer J.: Phosphorus flame retardants: Properties, production, environmental occurrence, toxicity and analysis. Chemosphere, 88, 1119–1153 (2012).

https://doi.org/10.1016/j.chemosphere.2012.03.067

- [22] Kim N. K., Dutta S., Bhattacharyya D.: A review of flammability of natural fibre reinforced polymeric composites. Composites Science and Technology, 162, 64– 78 (2018).
  - https://doi.org/10.1016/j.compscitech.2018.04.016
- [23] Costes L., Laoutid F., Brohez S., Dubois P.: Bio-based flame retardants: When nature meets fire protection. Materials Science and Engineering R: Reports, 117, 1–25 (2017).
  - https://doi.org/10.1016/j.mser.2017.04.001
- [24] Zhao P., Guo C., Li L.: Exploring the effect of melamine pyrophosphate and aluminum hypophosphite on flame retardant wood flour/polypropylene composites. Construction and Building Materials, 170, 193– 199 (2018).
  - https://doi.org/10.1016/j.conbuildmat.2018.03.074
- [25] Naik A. D., Fontaine G., Samyn F., Delva X., Bourgeois Y., Bourbigot S.: Melamine integrated metal phosphates as non-halogenated flame retardants: Synergism with aluminium phosphinate for flame retardancy in glass fiber reinforced polyamide 66. Polymer Degradation and Stability, 98, 2653–2662 (2013). https://doi.org/10.1016/j.polymdegradstab.2013.09.029
- [26] Li Y., Xue B., Wang S., Sun J., Li H., Gu X., Wang H., Zhang S.: Photoaging and fire performance of polypropylene containing melamine phosphate. ACS Applied Polymer Materials, 2, 4455–4463 (2020). https://doi.org/10.1021/acsapm.0c00578
- [27] Barczewski M., Hejna A., Andrzejewski J., Aniśko J., Piasecki A., Mróz A., Ortega Z., Rutkowska D., Sałasińska K.: The recyclability of fire-retarded biobased polyamide 11 (PA11) composites reinforced with basalt fibers (BFs): The influence of reprocessing on structure, properties, and fire behavior. Molecules, 29, 3233 (2024).
  - https://doi.org/10.3390/molecules29133233
- [28] Lv P., Wang Z., Hu K., Fan W.: Flammability and thermal degradation of flame retarded polypropylene composites containing melamine phosphate and pentaery-thritol derivatives. Polymer Degradation and Stability, 90, 523–534 (2005).
  - https://doi.org/10.1016/j.polymdegradstab.2005.04.003
- [29] Zhou S., Wang Z., Gui Z., Hu Y.: Flame retardation and thermal degradation of flame-retarded polypropylene composites containing melamine phosphate and pentaerythritol phosphate. Fire and Materials, **32**, 307–319 (2008).
  - https://doi.org/10.1002/fam.969
- [30] Wang Z., Qu B., Fan W., Huang P.: Combustion characteristics of halogen-free flame-retarded polyethylene containing magnesium hydroxide and some synergists. Journal of Applied Polymer Science, **81**, 206–214 (2001).
  - https://doi.org/10.1002/app.1430

- [31] Pan L. L., Li G. Y., Su Y. C., Lian J. S.: Fire retardant mechanism analysis between ammonium polyphosphate and triphenyl phosphate in unsaturated polyester resin. Polymer Degradation and Stability, **97**, 1801–1806 (2012).
  - https://doi.org/10.1016/j.polymdegradstab.2012.06.002
- [32] Wei M., Murphy D., Barry C., Mead J.: Halogen-free flame retardants for wire and cable applications. Rubber Chemistry and Technology, 83, 282–302 (2010). https://doi.org/10.5254/1.3525686
- [33] Paszkiewicz S., Irska I., Taraghi I., Piesowicz E., Sieminski J., Zawisza K., Pypeć K., Dobrzynska R., Terelak-Tymczyna A., Stateczny K., Szymczak B.: Halloysite nanotubes and silane-treated alumina trihydrate hybrid flame retardant system for high-performance cable insulation. Polymers, 13, 2134 (2021). https://doi.org/10.3390/polym13132134
- [34] Shang K., Lin G-D., Jiang H-J., Jin X., Zhao J., Liu D., Zhao B., Yang J-J., Fu T., Wang J-S.: Flame retardancy, combustion, and ceramization behavior of ceramifiable flame-retardant room temperature vulcanized silicone rubber foam. Fire and Materials, 47, 1082–1091 (2023). https://doi.org/10.1002/fam.3154
- [35] Sałasińska K., Barczewski M., Kirpluks M., Pomilovskis R., Sulima P., Michałowski S., Mietliński P., Przyborowski J. A., Boczkowska A.: Bio-based flameretardant systems for polymers obtained *via* Michael 1,4-addition. Molecules, 30, 2556 (2025). https://doi.org/10.3390/molecules30122556
- [36] Sałasińska K., Ortega Z., Jurczyk-Kowalska M., Borowicz M., Misiak M., Rutkowska D., Strycharz K., Cygan T., Paciorek-Sadowska J., Barczewski M.: Biosourced flame retardant systems for polymers: The influence of chemical modification of giant reed on thermal stability and flammability of PA11. Journal of Thermal Analysis and Calorimetry, in press (2025). https://doi.org/10.1007/s10973-025-14375-6
- [37] Velencoso M. M., Battig A., Markwart J. C., Schartel B., Wurm F. R.: Molecular firefighting How modern phosphorus chemistry can help solve the challenge of flame retardancy. Angewandte Chemie International Edition, 57, 10450–10467 (2018). https://doi.org/10.1002/anie.201711735
- [38] Lanyi F. J., Wenzke N., Kaschta J., Schubert D. W.: On the determination of the enthalpy of fusion of α-crystalline isotactic polypropylene using differential scanning calorimetry, X-ray diffraction, and Fourier-transform infrared spectroscopy: An old story revisited. Advanced Engineering Materials, 22, 1900796 (2020). https://doi.org/10.1002/adem.201900796
- [39] Jyoti J., Singh B. P., Arya A. K., Dhakate S. R.: Dynamic mechanical properties of multiwall carbon nanotube reinforced ABS composites and their correlation with entanglement density, adhesion, reinforcement and C factor. RSC Advances, 6, 3997–4006 (2016). https://doi.org/10.1039/C5RA25561A

- [40] Gopanna A., Mandapati R. N., Thomas S. P., Rajan K., Chavali M.: Fourier transform infrared spectroscopy (FTIR), Raman spectroscopy and wide-angle X-ray scattering (WAXS) of polypropylene (PP)/cyclic olefin copolymer (COC) blends for qualitative and quantitative analysis. Polymer Bulletin, **76**, 4259–4274 (2019). https://doi.org/10.1007/s00289-018-2599-0
- [41] Amariei G., Henriksen M. L., Klarskov P., Hinge M.: Quantification of aluminium trihydrate flame retardant in polyolefins *via* in-line hyperspectral imaging and machine learning for safe sorting. Spectrochimica Acta Part A: Molecular and Biomolecular Spectroscopy, **311**, 123984 (2024).

https://doi.org/10.1016/j.saa.2024.123984

[42] González-Gómez M. A., Belderbos S., Yañez-Vilar S., Piñeiro Y., Cleeren F., Bormans G., Deroose C. M., Gsell W., Himmelreich U., Rivas J.: Development of superparamagnetic nanoparticles coated with polyacrylic acid and aluminum hydroxide as an efficient contrast agent for multimodal imaging. Nanomaterials, 9, 1626 (2019).

https://doi.org/10.3390/nano9111626

- [43] Zhu L., Pu S., Lu F., Liu K., Zhu T., Li J., Li J.: Preparation of dispersed aluminum hydroxide nanoparticles *via* non-aqueous route and surface modification. Materials Chemistry and Physics, **135**, 979–984 (2012). <a href="https://doi.org/10.1016/j.matchemphys.2012.06.002">https://doi.org/10.1016/j.matchemphys.2012.06.002</a>
- [44] Dao K. C.: Rubber phase dispersion in polypropylene. Polymer, **25**, 1527–1533 (1984). https://doi.org/10.1016/0032-3861(84)90121-6
- [45] Lendvai L.: A novel preparation method of polypropylene/natural rubber blends with improved toughness. Polymer International, **70**, 298–307 (2021). https://doi.org/10.1002/pi.6133
- [46] Chandran N., Sarathchandran C., Sivadas A., Thomas S.: Interfacial interaction in polypropylene-natural rubber blends: Role of natural rubber on morphological, rheological, and mechanical evolution. Journal of Polymer Research, 29, 24 (2022). https://doi.org/10.1007/s10965-021-02873-8
- [47] Vijayan D., Mathiazhagan A., Joseph R.: Aluminium trihydroxide: Novel reinforcing filler in polychloroprene rubber. Polymer, **132**, 143–156 (2017). https://doi.org/10.1016/j.polymer.2017.10.058
- [48] Shah A. ur R., Lee D-W., Wang Y-Q., Wasy A., Ham K. C., Jayaraman K., Kim B-S., Song J-I.: Effect of concentration of ATH on mechanical properties of polypropylene/aluminium trihydrate (PP/ATH) composite. Transactions of Nonferrous Metals Society of China, 24, s81–s89 (2014). https://doi.org/10.1016/S1003-6326(14)63292-1
- [49] Parida M. R., Mohanty S., Biswal M., Nayak S. K., Rai S.: Influence of aluminum trihydrate (ATH) particle size on mechanical, thermal, flame retardancy and combustion behavior of polypropylene composites. Journal of Thermal Analysis and Calorimetry, 148, 807–819

https://doi.org/10.1007/s10973-022-11851-1

- [50] Hippi U., Mattila J., Korhonen M., Seppälä J.: Compatibilization of polyethylene/aluminum hydroxide (PE/ATH) and polyethylene/magnesium hydroxide (PE/MH) composites with functionalized polyethylenes. Polymer, **44**, 1193–1201 (2003). https://doi.org/10.1016/S0032-3861(02)00856-X
- [51] Chen X., Yu J., Guo S., Lu S., Luo Z., He M.: Surface modification of magnesium hydroxide and its application in flame retardant polypropylene composites. Journal of Materials Science, 44, 1324–1332 (2009). https://doi.org/10.1007/s10853-009-3273-6
- [52] Zhang X., Guo F., Chen J., Wang G., Liu H.: Investigation of interfacial modification for flame retardant ethylene vinyl acetate copolymer/alumina trihydrate nanocomposites. Polymer Degradation and Stability, 87, 411–418 (2005).

https://doi.org/10.1016/j.polymdegradstab.2004.08.013

[53] Pracella M., Haque Md. M-U., Alvarez V.: Functionalization, compatibilization and properties of polyolefin composites with natural fibers. Polymers, 2, 554–574 (2010).

https://doi.org/10.3390/polym2040554

[54] Sutar H., Sahoo P. C., Sahu P. S., Sahoo S., Murmu R., Swain S., Mishra S. C.: Mechanical, thermal and crystallization properties of polypropylene (PP) reinforced composites with high density polyethylene (HDPE) as matrix. Materials Sciences and Applications, 09, 502–515 (2018).

https://doi.org/10.4236/msa.2018.95035

- [55] Lima P. S., Oliveira J. M., Costa V. A. F.: Crystallization kinetics of thermoplastic elastomeric blends based on ground tyre rubber. Journal of Applied Polymer Science, 132, 42589 (2015).
  - https://doi.org/10.1002/app.42589
- [56] Seshweni M. H. E., Makhatha M. E., Botlhoko O. J., Obadele B. A., Vijayan V., Chiniwar D. S., Kumar P., Vishwanatha M. V.: Evaluation of mechanical and thermal properties of polypropylene-based nanocomposites reinforced with silica nanofillers *via* melt processing followed by injection molding. Journal of Composites Science, 7, 520 (2023).

https://doi.org/10.3390/jcs7120520

- [57] Dziadowiec D., Matykiewicz D., Szostak M., Andrzejewski J.: Overview of the cast polyolefin film extrusion technology for multi-layer packaging applications. Materials, 16, 1071 (2023). https://doi.org/10.3390/ma16031071
- [58] Li J., Shanks R. A., Olley R. H., Greenway G. R.: Miscibility and isothermal crystallisation of polypropylene in polyethylene melts. Polymer, **42**, 7685–7694 (2001). https://doi.org/10.1016/S0032-3861(01)00248-8
- [59] Fazli A., Rodrigue D.: Effect of ground tire rubber (GTR) particle size and content on the morphological and mechanical properties of recycled high-density polyethylene (rHDPE)/GTR blends. Recycling, 6, 44 (2021).

https://doi.org/10.3390/recycling6030044

- [60] Chang E. P.: Crystallization studies on fire-retardant polypropylene. Journal of Applied Polymer Science, **21**, 937–942 (1977).
  - $\underline{https://doi.org/10.1002/app.1977.070210406}$
- [61] Mysiukiewicz O., Sałasińska K., Barczewski M., Celiński M., Skórczewska K.: Effect of intumescent flame retardants on non-isothermal crystallization behavior of high-density polyethylene. Polymer Engineering and Science, 62, 2230–2242 (2022). https://doi.org/10.1002/pen.26003
- [62] Cui L., Wang P., Zhang Y., Zhang L., Chen Y., Wang L., Liu L., Guo X.: Combined effect of α-nucleating agents and glass fiber reinforcement on a polypropylene composite: A balanced approach. RSC Advances, 7, 42783–42791 (2017). https://doi.org/10.1039/C7RA08322J
- [63] de Miranda L. F., Silveira L. H., Silva L. G. A., Munhoz Jr. A. H.: Irradiation of a polypropilene-glass fiber composite. Advances in Science and Technology, 71, 138– 144 (2010).
  - https://doi.org/10.4028/www.scientific.net/AST.71.138
- [64] Watt E., Abdelwahab M. A., Snowdon M. R., Mohanty A. K., Khalil H., Misra M.: Hybrid biocomposites from polypropylene, sustainable biocarbon and graphene nanoplatelets. Scientific Reports, 10, 10714 (2020). https://doi.org/10.1038/s41598-020-66855-4
- [65] Snowdon M. R., Mohanty A. K., Misra M.: Miscibility and performance evaluation of biocomposites made from polypropylene/poly(lactic acid)/poly(hydroxybutyrate-co-hydroxyvalerate) with a sustainable biocarbon filler. ACS Omega, 2, 6446–6454 (2017). https://doi.org/10.1021/acsomega.7b00983
- [66] Abdelwahab M. A., Rodriguez-Uribe A., Misra M. K., Mohanty A.: Injection molded novel biocomposites from polypropylene and sustainable biocarbon. Molecules, 24, 4026 (2019).
  - https://doi.org/10.3390/molecules24224026
- [67] Luna C. B. B., da Silva F. S., da Silva Barbosa Ferreira E., da Silva A. L., Wellen R. M. R., Araújo E. M.: Transforming vulcanized styrene–butadiene waste into valuable raw material: An opportunity for high-impact polypropylene production. Polymer Bulletin, **81**, 423–447 (2024).
  - $\underline{https://doi.org/10.1007/s00289\text{-}023\text{-}04729\text{-}1}$
- [68] Wang X., Hu S., Guo Y., Li G., Xu R.: Toughened highflow polypropylene with polyolefin-based elastomers. Polymers, 11, 1976 (2019). https://doi.org/10.3390/polym11121976
- [69] Andrzejewski J., Michałowski S.: Development of a new type of flame retarded biocomposite reinforced with a biocarbon/basalt fiber system: A comparative study between poly(lactic acid) and polypropylene. Polymers, 14, 4086 (2022). https://doi.org/10.3390/polym14194086

- [70] Andrzejewski J., Marciniak-Podsadna L.: Development of thermal resistant FDM printed blends. The preparation of GPET/PC blends and evaluation of material performance. Materials, 13, 2057 (2020). https://doi.org/10.3390/ma13092057
- [71] Wong A. C-Y.: Heat deflection characteristics of polypropylene and polypropylene/polyethylene binary systems. Composites Part B: Engineering, 34, 199–208 (2003). https://doi.org/10.1016/S1359-8368(02)00080-X
- [72] Panthapulakkal S., Sain M.: Injection-molded short hemp fiber/glass fiber-reinforced polypropylene hybrid composites – Mechanical, water absorption and thermal properties. Journal of Applied Polymer Science, 103,
  - https://doi.org/10.1002/app.25486

2432-2441 (2007).

- [73] Deng S., Hou M., Ye L.: Temperature-dependent elastic moduli of epoxies measured by DMA and their correlations to mechanical testing data. Polymer Testing, 26, 803–813 (2007).
  - https://doi.org/10.1016/j.polymertesting.2007.05.003
- [74] Kościuszko A., Sykutera D., Czyżewski P., Hoyer S., Kroll L., Szczupak B.: Processing and mechanical properties of highly filled PP/GTR compounds. Materials, 15, 3799 (2022).
  - https://doi.org/10.3390/ma15113799
- [75] Grala M., Bartczak Z., Różański A.: Morphology, thermal and mechanical properties of polypropylene/SiO<sub>2</sub> nanocomposites obtained by reactive blending. Journal of Polymer Research, 23, 25 (2016). https://doi.org/10.1007/s10965-015-0914-0
- [76] Boyd R. H.: Relaxation processes in crystalline polymers: Experimental behaviour A review. Polymer, **26**, 323–347 (1985).
  - https://doi.org/10.1016/0032-3861(85)90192-2
- [77] Khanna Y. P., Turi E. A., Taylor T. J., Vickroy V. V., Abbott R. F.: Dynamic mechanical relaxations in polyethylene. Macromolecules, **18**, 1302–1309 (1985). https://doi.org/10.1021/ma00148a045
- [78] Krumbholz N., Hochrein T., Vieweg N., Hasek T., Kretschmer K., Bastian M., Mikulics M., Koch M.: Monitoring polymeric compounding processes inline with THz time-domain spectroscopy. Polymer Testing, 28, 30–35 (2009).
  - https://doi.org/10.1016/j.polymertesting.2008.09.009
- [79] Salazar-Cruz B. A., Chávez-Cinco M. Y., Morales-Cepeda A. B., Ramos-Galván C. E., Rivera-Armenta J. L.: Evaluation of thermal properties of composites prepared from pistachio shell particles treated chemically and polypropylene. Molecules, 27, 426 (2022). https://doi.org/10.3390/molecules27020426
- [80] Bashir M. A.: Use of dynamic mechanical analysis (DMA) for characterizing interfacial interactions in filled polymers. Solids, 2, 108–120 (2021). https://doi.org/10.3390/solids2010006

- [81] Bagotia N., Sharma D. K.: Systematic study of dynamic mechanical and thermal properties of multiwalled carbon nanotube reinforced polycarbonate/ethylene methyl acrylate nanocomposites. Polymer Testing, 73, 425–432 (2019).
  - https://doi.org/10.1016/j.polymertesting.2018.12.006
- [82] Shubhra Q. T. H., Alam A. K. M. M., Quaiyyum M. A.: Mechanical properties of polypropylene composites: A review. Journal of Thermoplastic Composite Materials, 26, 362–391 (2013). https://doi.org/10.1177/0892705711428659
- [83] Pape P. G., Plueddemann E. P.: Methods for improving the performance of silane coupling agents. Journal of Adhesion Science and Technology, 5, 831–842 (1991). https://doi.org/10.1163/156856191X00242
- [84] Voda A., Beck K., Schauber T., Adler M., Dabisch T., Bescher M., Viol M., Demco D. E., Blümich B.: Investigation of soft segments of thermoplastic polyurethane by NMR, differential scanning calorimetry and rebound resilience. Polymer Testing, 25, 203–213 (2006). <a href="https://doi.org/10.1016/j.polymertesting.2005.10.007">https://doi.org/10.1016/j.polymertesting.2005.10.007</a>
- [85] Raue F., Ehrenstein G. W.: Characterization of the dynamic properties of binary polypropylene blends via the hysteresis measurement method. Macromolecular Symposia, 148, 229–240 (1999). https://doi.org/10.1002/masy.19991480118
- [86] Sundaravadivel G., Venkataraman S. R., Vishvanathperumal S., Navaneethakrishnan V.: Influence of APTES modified HNTs on properties of NR/ EPDM nanocomposites. Silicon, 15, 6715–6727 (2023). https://doi.org/10.1007/s12633-023-02668-0
- [87] Paszkiewicz S., Irska I., Piesowicz E.: Modification of substandard EPDM with amorphous thermoplastic polyesters (PETG and PEF): Microstructure and physical properties. Polish Journal of Chemical Technology, 20, 8–14 (2018).
  - https://doi.org/10.2478/pjct-2018-0017

- [88] Gunes O. C., Gomek R., Tamar A., Kandemir O. K., Karaorman A., Albayrak A. Z.: Comparative study on flame retardancy, thermal, and mechanical properties of glass fiber reinforced polyester composites with ammonium polyphosphate, expandable graphite, and aluminum tri-hydroxide. Arabian Journal for Science and Engineering, 43, 6211–6218 (2018). https://doi.org/10.1007/s13369-018-3397-6
- [89] Liu Z., Chen J., Hua Y., Qian L., Sun J., Li H., Gu X., Zhang S.: Toward a deep understanding of the difference between isotactic and syndiotactic polypropylene on the fire performance and degradation behavior. Polymer Degradation and Stability, 206, 110195 (2022). https://doi.org/10.1016/j.polymdegradstab.2022.110195
- [90] Zhang X., Zhao Y., Zhang T., Ding Z., Li C., Lu S.: Characterization of thermal decomposition and combustion for commercial flame-retardant rubber floor cloth in TG-FTIR and FPA. Journal of Thermal Analysis and Calorimetry, 135, 3453–3461 (2019). https://doi.org/10.1007/s10973-018-7617-9
- [91] Sun L., Wen Y., Liu Q., Li D., Lyu L., Pei J., Zhang J., Li R.: A laboratory investigation into the effect of waste non-tire rubber particles on the performance properties of terminal blend rubberized asphalt binders. Construction and Building Materials, 313, 125409 (2021). https://doi.org/10.1016/j.conbuildmat.2021.125409
- [92] Tang X., Chen Z., Liu J., Chen Z., Xie W., Evrendilek F., Buyukada M.: Dynamic pyrolysis behaviors, products, and mechanisms of waste rubber and polyurethane bicycle tires. Journal of Hazardous Materials, 402, 123516 (2021). https://doi.org/10.1016/j.jhazmat.2020.123516
- [93] Schartel B., Hull T. R.: Development of fire-retarded materials Interpretation of cone calorimeter data. Fire and Materials, **31**, 327–354 (2007). https://doi.org/10.1002/fam.949
- [94] Günther M., Levchik S. V., Schartel B.: Bubbles and collapses: Fire phenomena of flame-retarded flexible polyurethane foams. Polymers for Advanced Technologies, 31, 2185–2198 (2020). https://doi.org/10.1002/pat.4939